

Weierstraß-Institut für Angewandte Analysis und Stochastik

im Forschungsverbund Berlin e.V.

Preprint

ISSN 0946 – 8633

Modelling of microstructure and its evolution in shape-memory-alloy single-crystals, in particular in CuAlNi

Martin Kružík^{1,2}, Alexander Mielke^{3,4} and Tomáš Roubíček^{5,1}

¹ Institute of Information Theory and Automation, Academy of Sciences,
Pod vodárenskou věží 4, CZ-18208 Praha 8, Czech Republic,

² Faculty of Civil Engineering, Czech Technical University, Thákurova 7,
CZ-166 29 Praha 6, Czech Republic,

³ Weierstraß-Institut für Angewandte Analysis und Stochastik, Mohren-
str.39, D-10117 Berlin, Germany,

⁴ Institut für Mathematik, Humboldt-Universität, Rudower Chaussee 23,
D-12489 Berlin, Germany,

⁵ Mathematical Institute, Charles University, Sokolovská 83,
CZ-186 75 Praha 8, Czech Republic.

submitted: 14 July 2005

No. 1047
Berlin 2005



2000 *Mathematics Subject Classification.* 35K85, 49S05, 74C15, 74N15.

Key words and phrases. Young measures, laminates, cubic-to-orthorhombic martensitic transformation, rate-independent evolution, energetic formulation, space-time discretization.

Edited by
Weierstraß-Institut für Angewandte Analysis und Stochastik (WIAS)
Mohrenstraße 39
10117 Berlin
Germany

Fax: + 49 30 2044975
E-Mail: preprint@wias-berlin.de
World Wide Web: <http://www.wias-berlin.de/>

Abstract

A continuum-mechanical description of the stored energy in shape-memory alloys is presented, with its multi-well character giving rise to a microstructure described, with a certain approximation, by special gradient Young measures. A rate-independent phenomenological dissipation is then considered to model a hysteretic response. Isothermal simulations with CuAlNi single crystal are presented.

1 Introduction

Shape-memory alloys (=SMAs) as so-called active (or smart) materials have been subjected to intensive theoretical and experimental research during the past decades, since they have been enjoying important applications in medicine and mechanical or aerospace engineering. They exhibit specific *hysteretic* stress/strain/temperature response, which is called *shape-memory effect*. This is related with the phenomenon that atoms tend to be arranged in different crystallographic configurations (in particular, having different symmetry groups) depending on temperature. Higher temperatures leads to a higher-symmetry (typically cubic) grid referred to as the *austenite* phase while lower temperature leads to a lower-symmetric grid (typically tetragonal, orthorhombic, monoclinic, or triclinic) called the *martensite* phase which may occur in M variants, $M=3,6,12$, or 4 in the mentioned cases, respectively. They can be combined coherently with each other, forming so-called *twins* of two variants, also called a *laminate*, cf. Figure 1d. Laminates can be combined in layers-within-layers to second-order (or even higher-order) laminates, cf. Figure 1e, or some other self-organization as wedges or branching like on Figure 1f can be observed and explained by mere crystallographic arguments, cf. [11, 12, 13, 31, 50, 56, 57]. These basic studies address primarily stress-free configurations. Under loading, one has to consider a phenomenological *free energy* recording energy, dependent on temperature and deformation gradient, stored in vibrating interatomic links. Under greater loading, austenite can usually transform to one (or rather more) variant(s) of martensite, which is referred to as a martensitic *phase transformation* (=PT) and leads to so-called *pseudo-elasticity* (sometimes also called *super-elasticity*). Under lower temperature, rather particular martensitic variants transform to each other, which is called re-orientation of martensite and gives rise to so-called *quasi-plasticity*. These processes are completely reversible but usually quite *dissipative*, i.e. mechanical energy transforms to heat (but, in closed cycles, without leading to any change of structure). These processes are *activated* (i.e. the related dissipation potential is nondifferentiable at that process rate = 0) and their dissipation is, with exception to fast and substantially anisothermal processes, *rate independent* (i.e. the dissipation potential is degree-1 homogeneous and the stress/strain response is *hysteretic*).

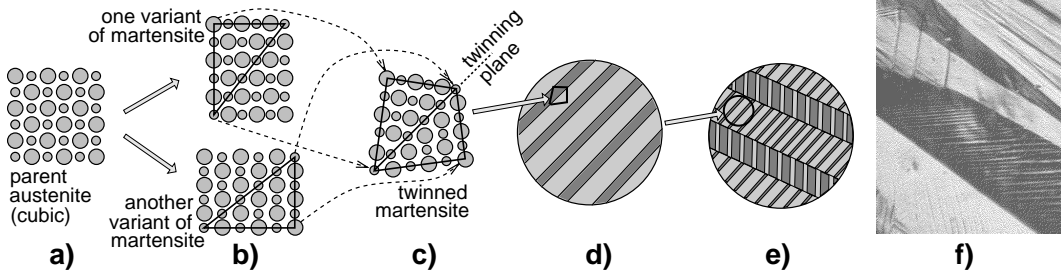


Fig. 1. Schematic explanation of the creation of twinned martensite and a real observation:

- a) the parent austenite (cubic),
- b) two variants of “orthorhombic” martensite elongated vertically or horizontally,
- c) twin occurring by matching two slightly rotated triangles of 2 martensitic variants,
- d) 1st-order laminate (the gray levels distinguish particular variants),
- e) 2nd-order laminate (layers within layers, cf. the rank-1 conditions (3)),
- f) a rather chaotic arrangement of martensite in a CuAlNi single crystal; courtesy of V. Novák and P. Šittner, Inst. of Physics, Acad. of Sciences of the Czech Rep.

Mathematical and computational modelling of SMAs represents a certain tool of theoretical understanding of PT processes. It may complete experimental results, may predict response of new materials, or may facilitate the usage of SMAs in engineering applications. The real situation in SMAs is truly *multi-scale* and creates a variety of possibilities for modelling, see [67] for a survey of a wide menagerie of SMA models ranging from nano- to macro-scales. Here we focus on a *mesoscopic* model based on *continuum mechanics* but involving, beside the macroscopic deformation and its gradients also volume fractions and their particular gradients. This seems a fruitful compromise allowing for modelling scales of large single crystals as often used in labs.

The goal of this article is to expose the “mesoscopic” description of the possible laminated microstructure by special so-called Young measures in Section 2 and the basic phenomenological concepts behind SMAs, i.e. the stored and dissipation energies, and the governing variational principles in Sections 3-4. Then, in Section 5, we present the evolution model together with its analysis involving some new mathematical results and eventually, in Section 6, we illustrate it on specific experiments with a specific SMA, namely CuAlNi which exhibits cubic-to-orthorhombic PT. We refer to [36, 68] for a simpler cubic-to-tetragonal PT occurring in NiMnGa, which is calculated by only 1st-order laminates. We will confine ourselves to isothermal processes in single-crystals, and intentionally suppress mathematical technicalities to minimum with a certain exception of Section 5.

2 Mesoscopic description of laminated microstructure as an approach to multiscale modelling

The stress-free parent austenite is a natural state of the material and, in the context of continuum mechanics, it is a natural *reference configuration* of a specimen occupying, say, a domain $\Omega \subset \mathbb{R}^3$. As usual, $y : \Omega \rightarrow \mathbb{R}^3$ denotes the *deformation* and $u : \Omega \rightarrow \mathbb{R}^3$ the *displacement*, related to each other by $y(x) = x + u(x)$, $x \in \Omega$. Hence the *deformation gradient* equals $F = \nabla y = \mathbb{I} + \nabla u$ with $\mathbb{I} \in \mathbb{R}^{3 \times 3}$ being the identity matrix and ∇ is the gradient operator.

As indicated on Fig. 1, the deformation gradient often tends to develop fast spatial oscillations which are due to non-(quasi)convexity of the stored energy density and which are difficult to be modelled in full detail, although some studies in this direction exists, too, cf. [3, 4]. We want to address a “mesoscopic” level

recording “limit information” of the faster and faster oscillating deformation gradient when we “zoom it out” towards the macroscopic scale. This can be described, at a current “macroscopic point” $x \in \Omega$, by a probability measure ν_x on the set of matrices from $\mathbb{R}^{3 \times 3}$; cf. e.g. [11, 12, 44, 50, 56]. The collection $\nu = \{\nu_x\}_{x \in \Omega}$ is called a *Young measure*; more precisely, the map $x \mapsto \nu_x$ is required to be still weakly measurable. In our context, relevant Young measures are only those that are attainable as a limit of gradients (in the sense of (57) below) of deformations $y \in W^{1,p}(\Omega; \mathbb{R}^3) := \{y \in L^p(\Omega; \mathbb{R}^3); \nabla y \in L^p(\Omega; \mathbb{R}^{3 \times 3})\}$, where $L^p(\Omega; \mathbb{R}^{3 \times 3}) := \{z : \Omega \rightarrow \mathbb{R}^{3 \times 3} \text{ measurable} : \int_{\Omega} |z|^p dx < +\infty\}$, for a suitable exponent $p \in (1, +\infty)$ related with the p -polynomial-type growth and coercivity of the stored energy density. Let us denote by $\mathcal{G}^p(\Omega; \mathbb{R}^{3 \times 3})$ the set of such parameterized measures. An example of a Young measure $\nu \in \mathcal{G}^p(\Omega; \mathbb{R}^{3 \times 3})$ describing a so-called 1st-order *laminate* (cf. Fig. 1d) with a underlying macroscopic deformation $y \in W^{1,p}(\Omega; \mathbb{R}^3)$ is

$$\nu = \{\nu_x\}_{x \in \Omega}, \quad \nu_x = \xi_0(x)\delta_{F_1(x)} + (1-\xi_0(x))\delta_{F_2(x)}, \quad (1a)$$

$$[\xi_0 F_1 + (1-\xi_0)F_2](x) = \nabla y(x), \quad F_1(x) - F_2(x) = a_0(x) \otimes n_0(x), \quad (1b)$$

$$0 \leq \xi_0(x) \leq 1, \quad a_0(x), n_0(x) \in \mathbb{R}^3. \quad (1c)$$

This process can be re-iterated: a 2nd-order laminate (cf. Fig. 1e) with the macroscopic deformation y as above is $\nu = \{\nu_x\}_{x \in \Omega}$, where

$$\begin{aligned} \nu_x = & \xi_0(x)\xi_1(x)\delta_{F_1(x)} + \xi_0(x)(1-\xi_1(x))\delta_{F_2(x)} \\ & + (1-\xi_0(x))\xi_2(x)\delta_{F_3(x)} + (1-\xi_0(x))(1-\xi_2(x))\delta_{F_4(x)}, \end{aligned} \quad (2)$$

with (dropping for simplicity a dependence on x)

$$F_1 - F_2 = a_1 \otimes n_1, \quad F_3 - F_4 = a_2 \otimes n_2, \quad (3a)$$

$$\xi_1 F_1 + (1-\xi_1)F_2 - \xi_2 F_3 - (1-\xi_2)F_4 = a_0 \otimes n_0, \quad (3b)$$

$$\nabla y = \xi_0 \xi_1 F_1 + \xi_0 (1-\xi_1) F_2 + (1-\xi_0) \xi_2 F_3 + (1-\xi_0) (1-\xi_2) F_4 \quad (3c)$$

and $0 \leq \xi_i \leq 1$, $a_i, n_i \in \mathbb{R}^3$, $i \in \{0, 1, 2\}$. Analogously, we can get laminates of an arbitrary order which are often called sequential laminates.

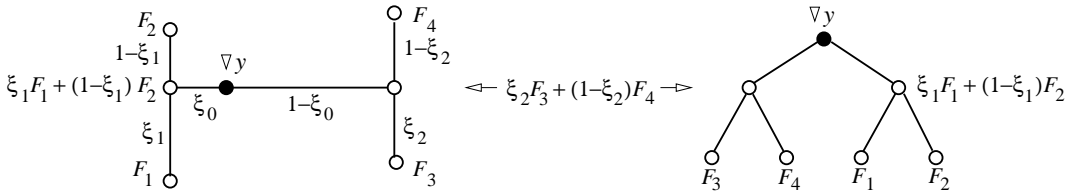


Fig. 2. Schematic graph with attributed edges (left), being in fact a binary tree (right), which corresponds to the 2nd-order laminate from (3).

Unfortunately, not every $\nu \in \mathcal{G}^p(\Omega; \mathbb{R}^{3 \times 3})$ is of the form of a sequential laminate, or even cannot be attained by sequential laminates, which can be interpreted that microstructures might be much more chaotic; this might be partly related with Fig. 1f. Although some explanation by wedge-like or other type of microstructures suggested by Bhattacharya [13] can be more adequate here. This might be connected with the

Šverák’s famous counterexample [76] that rank-one convexity does not imply quasi-convexity. Moreover, an efficient description of $\mathcal{G}^p(\Omega; \mathbb{R}^{3 \times 3})$ is not available, which is related with lack of a local characterization of quasiconvex functions; cf. [33].

Starting from 1D-numerical experiments by Nicolaides and Walkington [53], there are numerical studies involving gradient Young measures as e.g. [5, 34, 35, 64] but, due to the mentioned impossibility of an efficient description of the whole set $\mathcal{G}^p(\Omega; \mathbb{R}^{3 \times 3})$, they eventually have to deal with laminates of an order $\kappa \geq 1$, let us denote this set as

$$\mathcal{G}_{\text{lam}}^{p,\kappa}(\Omega; \mathbb{R}^{3 \times 3}) := \{ \nu \in \mathcal{G}^p(\Omega; \mathbb{R}^{3 \times 3}); \nu_x \text{ is a } \kappa\text{-order laminate for a.a. } x \in \Omega \}. \quad (4)$$

Nevertheless, laminates enable us to describe volume fractions of particular phases/variants at a given material point. The idea of looking at volume fractions (sometimes in simplified situations leading to a transformation strain as an independent variable) occurred in various other models, too, see Frémond [21, 22], Auricchio et al. [7, 8], LExcellent et al. [39, 80], or Patoor et al. [55], Souza et al. [73], often meant for polycrystals so that the fine (and in context of single-crystals very important) issues related with rank-one connections are often not accounted for.

3 Stored energy and its minimization

The specific energy stored in the inter-atomic links in the continuum $\hat{\varphi} = \hat{\varphi}(F)$ is phenomenologically described as a function of the deformation gradient F ; recall that we consider temperature constant. The *frame-indifference*, i.e. $\hat{\varphi}(F) = \hat{\varphi}(RF)$ for any $R \in \text{SO}(3)$, the group of orientation-preserving rotations, requires that $\hat{\varphi}$ in fact depends only on the (right) *Cauchy-Green stretch* tensor $C := F^\top F$. As $F = \mathbb{I} + \nabla u$, we can express the specific stored energy in terms of the displacement gradient as

$$\varphi = \varphi(\nabla u) = \hat{\varphi}(\mathbb{I} + \nabla u). \quad (5)$$

The absence of an explicit dependence on x is related to homogenous single crystals considered. The *Piola-Kirchhoff stress* $\sigma : \mathbb{R}^{3 \times 3} \rightarrow \mathbb{R}^{3 \times 3}$ is given by $\sigma = \varphi'(\nabla u)$ with φ' denoting the tensor-valued gradient.

We will use a *St. Venant-Kirchhoff*-like form of the stored energy of each particular phase variants which allows for an explicit reference to measured data and can easily be applied to various materials. We consider M variants of martensite determined, in the stress-free state, by *distortion matrices* U_ℓ , $\ell = 1, \dots, M$, while the cubic austenite corresponds to $U_0 = \mathbb{I}$.

The frame-indifferent stored energy of particular phases or phase variants is considered as a function of the *Green strain* tensor ε^ℓ related to the distortion of this phase (variant). In the simplest case (cf. [57, Sect.6.6], e.g.), one can consider a function quadratic in terms of ε^ℓ of the form

$$\hat{\varphi}_\ell(F) = \frac{1}{2} \sum_{i,j,k,l=1}^d \varepsilon_{ij}^\ell \mathcal{C}_{ijkl}^\ell \varepsilon_{kl}^\ell + d_\ell, \quad \varepsilon^\ell = \frac{R_\ell^\top (U_\ell^\top)^{-1} F^\top F U_\ell^{-1} R_\ell - \mathbb{I}}{2}, \quad (6)$$

where $\mathcal{C}^\ell = \{\mathcal{C}_{ijkl}^\ell\}$ is the 4th-order tensor of elastic moduli satisfying the usual symmetry relations depending also on symmetry of the specific phase (variant) ℓ , d_ℓ is some offset; d_ℓ depends on temperature which is, however, considered as fixed – this dependence differs in various phases due to various heat capacities, which

is just what makes the shape-memory effect. (The temperature dependence of the elastic tensors \mathcal{C}^ℓ and the distortion matrices U_ℓ is usually negligible.) Finally, R_ℓ is a rotation matrix transforming the basis of the austenite to the basis of the martensitic variant ℓ , if $\ell \geq 1$, cf. (73) below, while $R_0 = \mathbb{I}$. We will advantageously use it to work with the same tensor of elastic moduli for all martensitic variants, contrary to an alternative method by Auld [6] which modifies the tensor \mathcal{C}^ℓ for each particular martensitic variant.

The simplest way to assembly the overall *multi-well* stored energy $\hat{\varphi}$ relying on that materials naturally tend to minimize stored energy is to put

$$\hat{\varphi} := \min_{\ell=0,\dots,M} \hat{\varphi}_\ell \quad (7)$$

although some statistical-physics based formula (with quite the same effect) can be consider, too; cf. [36, 67, 68].

The total stored energy in the bulk occupying, in its reference configuration, the domain Ω is then

$$V(u) := \int_{\Omega} \varphi(\nabla u) \, dx. \quad (8)$$

Basic variational principle (although not always followed, cf. Section 4) is *minimization of the stored energy*. Due to the multi-well character φ and here also due to the chosen St.Venant-Kirchhoff form of φ , minimizing sequences of V tend to develop, in general, faster and faster spatial oscillations of their gradients, which is related to development of the finer and finer microstructures when the stored energy is to be minimized, cf. again Fig. 1d–f. The minimum of V , under specific boundary conditions for u , say

$$u|_{\Gamma_D} = u_D \quad (9)$$

where Γ_D is a part of the (Lipschitz) boundary $\partial\Omega$ of Ω , need not ever be attained on the space $W^{1,p}(\Omega; \mathbb{R}^3)$, however. This effect is due to neglecting the (usually small) energy stored in the interfaces like the twinning plane on Fig. 1c, which is certainly relevant approach on meso- and macroscopic level. However, the minimum is attained, under suitable coercivity conditions, on Young measures from Section 2. For this, we need to extend V by continuity for such measures. Considering now the configuration as the couple $(u, \nu) \in W^{1,p}(\Omega; \mathbb{R}^3) \times \mathcal{G}^p(\Omega; \mathbb{R}^{3 \times 3})$, the extended functional is

$$\bar{V}(u, \nu) := \int_{\Omega} \int_{\mathbb{R}^{3 \times 3}} \varphi(A) \nu_x(dA) dx = \int_{\Omega} \int_{\mathbb{R}^{3 \times 3}} \hat{\varphi}(\mathbb{I} + A) \nu_x(dA) dx. \quad (10)$$

The set of admissible configurations is now

$$\left\{ (u, \nu) \in W^{1,p}(\Omega; \mathbb{R}^3) \times \mathcal{G}^p(\Omega; \mathbb{R}^{3 \times 3}); \text{ (9) holds and } \int_{\mathbb{R}^{3 \times 3}} A \nu_x(dA) = \nabla u \text{ for a.a. } x \in \Omega \right\}, \quad (11)$$

and the minimum of \bar{V} on this set is the infimum of V on $W^{1,p}(\Omega; \mathbb{R}^3)$ under (9). The process of extension V to \bar{V} is called *relaxation*, cf. [56, 64].

4 Dissipation energy and its maximization

PT in SMAs is, to a large extent, a *rate-independent, activated process* and leads to a specific dissipation which results in a hysteretic response in stress/strain diagrams. Its modelling is equally important as the stored energy but the related phenomenology is still less understood than the stored-energy one; indeed, as pointed out by Bhattacharya et al. [15], ‘much remains unknown concerning the nucleation and evolution of microstructure, and the resultant hysteresis’. Let us recall that the orbits $\text{SO}(3)U_\ell$ and $\text{SO}(3)U_l$ are *rank-1 connected* if

$$\exists R \in \text{SO}(3) : \quad \text{Rank}(U_\ell - RU_l) = 1; \quad (12)$$

cf. also Fig.1b,c. There seems to be two main approaches to the dissipation problem:

- (A) the hysteresis (and the related rate-independent dissipation) is determined by the stored-energy landscape, advocated essentially by Abeyaratne, Knowles [2], Ball et al. [9, 10], Goldstein [23], James and Zhang [32], Šilhavý [70], Truskinovsky [78], Vainchtein, and Rosakis [79], etc. The common philosophy is that, if the orbits $\text{SO}(3)U_\ell$ and $\text{SO}(3)U_l$ are rank-1 connected, then the dissipation within PT between these (phase) variants is small, or rather zero, otherwise it is related with metastability and a stress which the material must inevitably withstand to move out of the bottoms of the wells during the PT.
- (B) The hysteresis is quite independent of the stored energy and needs a separate phenomenology (recording, e.g, various impurities and dislocations in the atomic grid that lead to bigger dissipation), advocated essentially (besides authors’ own previous works) by Auricchio et al. [7, 8], Frémond [21], Govindjee, Hall, [25, 28] and Miehe [24, 26], Hackl et al. [27], LExcellent et al. [39, 80], Rajagopal, Srinivasa [60], Souza [73], Stupkiewicz, Petryk [74], and many others.

It is likely that both these approaches combine mutually. Besides, for completeness let us mention that there are attempts to apply a phenomenology like (B) but through a modification of the stored energy which then causes a hysteresis like in the case (A), see Abeyaratne, Chu, James [1], Müller, Xu [49], or Wilmski [81].

Following [65, Formula (33)] and the works [4, 36, 45, 58, 59, 66, 67, 68], we adopt a (to some extent quite simplified) standpoint that the amount of dissipated energy within the particular PT between austenite and a martensitic variant or between two martensitic variants can be described by a specific energy (of the dimension $\text{J/m}^3=\text{Pa}$). It has independently been adopted in physics, see [30, 77, 80]. For this, we need to identify the particular phases or phase variants and thus we define a continuous mapping $\mathcal{L} : \mathbb{R}^{3 \times 3} \rightarrow \Delta$ where

$$\Delta := \left\{ \zeta \in \mathbb{R}^{1+M} ; \zeta_\ell \geq 0, \ell = 0, \dots, M, \sum_{\ell=0}^M \zeta_\ell = 1 \right\} \quad (13)$$

is a simplex with $M+1$ vertexes, $M =$ the number of martensitic variants as in Section 3. As in (5), we assume

$$\mathcal{L}(\nabla u) = \hat{\mathcal{L}}(\mathbb{I} + \nabla u) \quad \text{with } \hat{\mathcal{L}} : \mathbb{R}^{3 \times 3} \rightarrow \Delta. \quad (14)$$

Here $\hat{\mathcal{L}}$ is related with the material itself and thus is to be frame indifferent. We assume, beside $\hat{\mathcal{L}}_\ell \geq 0$ and $\sum_{\ell=0}^M \hat{\mathcal{L}}_\ell = 1$, that $\hat{\mathcal{L}}_\ell(F) = 1$ if F is in the ℓ -th

(phase) variant, i.e. F is in a vicinity of ℓ -th well $\text{SO}(3)U_\ell$ of φ , which can be identified according to the stretch tensor $F^\top F$ close to $U_\ell^\top U_\ell$, cf. [46, 48] and the formula (74) below. If $\hat{\mathcal{L}}(F)$ is not in any vertex of Δ , then it means that F in the spinodal region where no definite (phase) variant is specified; we assume, however, that the wells are sufficiently deep and the (phase) variants geometrically sufficiently far from each other that the tendency for minimization of the stored energy will essentially prevent F to range the spinodal region and thus the concrete form of $\hat{\mathcal{L}}$ does not seem to be important as long as $\hat{\mathcal{L}}$ enjoys the above properties. Hence \mathcal{L} plays the role of what is often called a vector of *order parameters* or a vector-valued *internal variable*.

The dissipation-energy phenomenology itself is considered through the choice of a “norm” on \mathbb{R}^{1+M} (not necessarily Euclidean and even not symmetric), let us denote it by $|\cdot|_M$; its physical dimension will be $\text{J/m}^3 = \text{Pa}$. The desired meaning is to set up the specific energy \mathcal{E}_ℓ needed for PT of a phase (variant) ℓ to l as $|e_\ell - e_l|_M$, where $e_\ell = (0, \dots, 0, 1, 0, \dots, 0) \in \mathbb{R}^{1+M}$ is the unit vector with 1 at the position ℓ . The set $\{\mathcal{E}_\ell\}_{\ell=0, \dots, M}$ can reflect both the presence/lack of rank-one connections (A) and the influence of various impurities (B).

Referring to a mesoscopic description through a Young measure $\nu \in \mathcal{G}^p(\Omega; \mathbb{R}^{3 \times 3})$, see Section 2, the *mesoscopic volume fractions* $\lambda = \lambda(x)$ at a current “macroscopic” point x is then

$$\lambda(x) := \int_{\mathbb{R}^{3 \times 3}} \mathcal{L}(A) \nu_x(\mathrm{d}A) = \int_{\mathbb{R}^{3 \times 3}} \hat{\mathcal{L}}(\mathbb{I} + A) \nu_x(\mathrm{d}A). \quad (15)$$

As a *mesoscopic configuration*, we will consider a triple $q = (u, \nu, \lambda)$, i.e. the macroscopic displacement, the Young measure describing the microstructure, and the volume fraction field; of course, they are linked with each other by (15) and also by the constraint in (11). In terms of $\frac{\mathrm{d}}{\mathrm{d}t}q$, the (pseudo) potential of dissipative forces R that corresponds to this phenomenology is

$$R\left(\frac{\mathrm{d}q}{\mathrm{d}t}\right) = R\left(\frac{\mathrm{d}u}{\mathrm{d}t}, \frac{\mathrm{d}\nu}{\mathrm{d}t}, \frac{\mathrm{d}\lambda}{\mathrm{d}t}\right) := \int_{\Omega} \left| \frac{\partial \lambda(t, x)}{\partial t} \right|_M \mathrm{d}x. \quad (16)$$

This means, considering a process over the time interval $[t_1, t_2]$, the overall dissipated energy by all undergone PTs in the whole specimen Ω will be

$$\int_{t_1}^{t_2} \int_{\Omega} \left| \frac{\partial \lambda}{\partial t} \right|_M \mathrm{d}x \mathrm{d}t = \int_{\Omega} \text{Var}_{t \in [t_1, t_2]} \lambda(t, x) \mathrm{d}x \quad (17)$$

where the total variation “Var” with respect to the (possibly nonsymmetric) norm $|\cdot|_M$ counts which PTs (and how many times) have been undergone at the point x . The important property of R is that it satisfies the triangle inequality, i.e.

$$\forall q_1, q_2, q_3 \in Q : \quad R(q_1 - q_3) \leq R(q_1 - q_2) + R(q_2 - q_3), \quad (18)$$

which follows immediately from convexity and the degree-1 homogeneity.

The dissipation mechanism through the convex, degree-1 homogeneous potential R is intimately related with Hill’s *maximum-dissipation principle* [29]. The desired energy balance, i.e. the rate of Helmholtz’ stored energy \bar{V} plus the dissipation rate equal to the power of the external force, is

$$\frac{\mathrm{d}\bar{V}}{\mathrm{d}t} + R\left(\frac{\mathrm{d}q}{\mathrm{d}t}\right) = \left\langle f, \frac{\mathrm{d}u}{\mathrm{d}t} \right\rangle \quad (19)$$

where the degree-1 homogeneous dissipation rate R can be written in the form

$$R\left(\frac{dq}{dt}\right) = \int_{\Omega} \omega(t, x) \cdot \frac{\partial \lambda(t, x)}{\partial t} dx \quad \text{with} \quad \omega(t, x) \in [\partial|\cdot|_M]\left(\frac{\partial \lambda(t, x)}{\partial t}\right) \quad (20)$$

with $\partial|\cdot|_M$ denoting the subdifferential of $|\cdot|_M$. The last inclusion can be written as

$$\left\langle \frac{\partial \lambda(t, x)}{\partial t}, \omega(t, x) \right\rangle = \max_{z \in Z} \left\langle \frac{\partial \lambda(t, x)}{\partial t}, z \right\rangle \quad \text{with} \quad Z := [\partial|\cdot|_M](0). \quad (21)$$

This says that, for the considered volume-fraction rate $\frac{\partial}{\partial t}\lambda$, the *driving stress* (or specific *activation energies*) ω in Pa (=J/m³) makes the dissipation caused by the PTs maximal among all other admissible driving stresses, i.e. those from the convex set $Z \subset \mathbb{R}^{1+M}$. In plasticity theory, this maximum-dissipation principle can alternatively be expressed as a normality in the sense that the *rate of plastic deformation belongs to the cone of outward normals to the elasticity domain*; see also [40, 71], and also [42] for the more general situation of standard generalized materials. Here, this would result in the observation that the rate $\frac{\partial}{\partial t}\lambda(t, x)$ of PTs at (t, x) belongs to the normal cone of the “elasticity domain” Z at the point $\omega(t, x)$. In particular, (21) says that $\frac{\partial}{\partial t}\lambda = 0$ (i.e. the volume fractions do not evolve) if $\omega(t, x)$ is inside Z (i.e. there is not enough stress to activate PTs at (t, x)). Also recall that ∂R is maximal responsive in the sense of [18]. For a discussion in a 1D-case see also [45, Remark 4.5]. However, we saw that (21) contains, in fact, only a rather small portion of information about the evolution and other principles can be considered at this context, too, cf. also Remark 5.4 below.

5 Energetic solution and its discretization

We want to present briefly the model of evolution of microstructure described “mesoscopically” as in Section 2 governed by the principles from Sections 3–4, as well as its mathematical analysis. It exploits the definition of the so-called energetic solution invented in [46, 47] (see also the survey article [44]) and the results are then mainly based on [36, 43, 45, 68] (improving substantially the results of [36, 68]) exploiting also some recent results from [20]. In accord with Section 6, we consider here a “soft-device” loading through time-varying Neumann’s boundary conditions.

We denote the set Q^0 of the admissible configurations q ’s, i.e.

$$\begin{aligned} Q^0 &= \{ (u, \nu, \lambda) \in Q ; \quad \lambda = \mathcal{L} \bullet \nu \text{ a.e.} \}, \quad \text{where} \quad (22) \\ Q &:= \left\{ q = (u, \nu, \lambda) \in W^{1,p}(\Omega; \mathbb{R}^3) \times \mathcal{G}^p(\Omega; \mathbb{R}^{3 \times 3}) \times L^1(\Omega; \mathbb{R}^{1+M}) ; \right. \\ &\quad \left. \nabla u(x) = \int_{\mathbb{R}^{3 \times 3}} A \nu_x(dA), \quad \lambda(x) \in \Delta \text{ a.e. on } \Omega, \quad u|_{\Gamma_D} = u_D \right\}, \end{aligned}$$

where we abbreviated

$$\lambda = \mathcal{L} \bullet \nu \quad \text{where} \quad [\mathcal{L} \bullet \nu](x) := \int_{\mathbb{R}^{3 \times 3}} \mathcal{L}(A) \nu_x(dA). \quad (23)$$

We distinguished, just for numerical purposes later, Q , which “forgets” the constraint $\lambda = \mathcal{L} \bullet \nu$, from Q_0 .

The Gibbs' stored energy which also counts for the time-dependent boundary conditions and which is regularized by $\rho > 0$ is

$$G(t, q) := G(t, u, \nu, \lambda) = \bar{V}(u, \nu) + \int_{\Gamma_N} f(t, x) \cdot u(x) \, dx + \rho |\lambda|_{\alpha, r}^r \text{ on } Q, \quad (24)$$

$$G^0(t, q) := \begin{cases} G(t, q) & \text{on } Q^0, \\ +\infty & \text{on } Q \setminus Q^0, \end{cases} \quad (25)$$

with \bar{V} from (10), $f : [0, T] \times \Gamma_N \rightarrow \mathbb{R}^3$ a prescribed "soft-device" loading, $\Gamma_N \subset \partial\Omega$, $T > 0$ a fixed time horizon, and with the semi-norm in the Sobolev-Slobodetskiĭ space $W^{\alpha, r}(\Omega; \mathbb{R}^{1+M})$ considered as

$$|\lambda|_{\alpha, r} := \left(\frac{1}{4} \int_{\Omega} \int_{\Omega} \frac{|\lambda(x) - \lambda(\tilde{x})|^r}{|x - \tilde{x}|^{3+r\alpha}} \, d\tilde{x} dx \right)^{1/r}, \quad (26)$$

for a fixed parameter $0 < \alpha < 1$. Such a regularizing term in (24) gives some (possibly very small) energy to spatial variation of mesoscopic volume fractions and is exploited for a rigorous proof of existence of energetic solutions as well as convergence of numerical approximations. Gradients of mesoscopic volume fractions have already been used in Frémond's model [21, p.364]. Our form (26) corresponds to the only " α -fractional gradient" which is compactifying, namely the embedding $W^{\alpha, r}(\Omega; \mathbb{R}^{1+M}) \subset L^1(\Omega; \mathbb{R}^{1+M})$ is compact. Also it allows for an element-wise affine approximation of λ , because $W^{\alpha, r}(\Omega; \mathbb{R}^{1+M}) \supset W^{1, \infty}(\Omega; \mathbb{R}^{1+M})$ or, if $\alpha < 1 - 3(r-1)/r$ with some $1 < r < 3/2$, for an element-wise constant approximation which has necessarily discontinuities on 2-dimensional manifolds requiring then $W^{\alpha, r}(\Omega; \mathbb{R}^{1+M}) \supset W^{1, 1}(\Omega; \mathbb{R}^{1+M})$; later in (33) we choose the latter option. In [45, 66] such a regularization was interpreted as a limit from the Ericksen-Timoshenko model scrutinized by Ren, Rogers, and Truskinovsky [61, 62] who also proposed a nonlocal term like (26) in the 1D case with either positive or also, for different purposes, non-positive kernels. One can interpret the energy (26) as associated to a sort of non-local microstress measuring nonlocal interactions related to spatial microstructural variations.

Definition 5.1 *The process $q : [0, T] \mapsto Q^0$ will be called an **energetic solution** to the problem given by the triple (G^0, R, q_0) , i.e. by the data $(\varphi, \mathcal{L}, |\cdot|_M, f, u_D, q_0, \rho)$, if it satisfies the initial condition $q(0) = q_0$, the static **stability condition**:*

$$\forall t \in [0, T] \quad \forall \tilde{q} \in Q^0 : \quad G^0(t, q(t)) \leq G^0(t, \tilde{q}) + R(\tilde{q} - q(t)), \quad (27)$$

and the **energy equality**

$$\forall s, t \in [0, T] : \quad G^0(t, q(t)) + \text{Var}_R(q; s, t) = G^0(s, q(s)) + \int_s^t \frac{\partial G^0}{\partial \vartheta}(\vartheta, q(\vartheta)) \, d\vartheta. \quad (28)$$

Here $\text{Var}_R(q; s, t)$ is the total variation of the process $q = (u, \nu, \lambda) : [0, T] \rightarrow Q$ over the time interval $[s, t]$ with respect to the norm $|\cdot|_M$, namely

$$\text{Var}_R(q; s, t) := \sup \sum_{i=1}^k R(q(t_i) - q(t_{i-1})) = \sup \sum_{i=1}^k \int_{\Omega} |\lambda(t_i, x) - \lambda(t_{i-1}, x)|_M \, dx \quad (29)$$

where the supremum is taken over all partition $s = t_0 < t_1 < \dots < t_k = t$, $k \in \mathbb{N}$. The definition of stability (27) and energy balance (28) could also be defined on all

of Q , since G^0 equals $+\infty$ on $Q \setminus Q^0$. It will be useful to define the *stability set* $\mathcal{S}^0(t)$ by

$$\mathcal{S}^0(t) := \{q \in Q; G^0(t, q) < +\infty, \forall \tilde{q} \in Q: G^0(t, q) \leq G^0(t, \tilde{q}) + R(\tilde{q} - q)\}. \quad (30)$$

Let us note that the stability (27) just means that $q(t) \in \mathcal{S}^0(t)$ for all $t \in [0, T]$.

Remark 5.2 The particular terms in (28) are Gibbs' energy at time t , the dissipated energy over the time interval $[s, t]$, the initial Gibbs' energy, and a (reduced) work of external loading over the time interval $[0, t]$. The adjective "reduced" refers to the by-part integration of the standard work of external loading $\int_0^t \int_{\Gamma_N} f(s, x) \cdot \frac{\partial}{\partial s} u \, dx ds$ which balances Helmholtz' (contrary to Gibbs') stored energy, cf. (19). This by-part integration is an essential trick because it allows, together with the definition (29), to omit any explicit reference to the time derivative $\frac{d}{dt}q$ in (27)–(28).

Remark 5.3 The energy balance (28) obviously produces no dissipation (i.e. no hysteresis on stress-strain diagrams) if $R = 0$. A similar effect occurs in usual viscosity/capillarity-type models if viscosity vanishes and enough capillarity (=gradients of enough higher-order in the stored energy) remains, cf. [59]. Here this effect is due to the regularizing term (26). Hence, incorporation of a dissipation even of type (A) (see Section 4) must be done in this model always through the dissipative-force potential R which may, in addition, involve some other phenomenology (see (B) in Section 4).

Remark 5.4 The energetic definition (27)–(28) is closely related to the so-called *doubly-nonlinear* evolution problem, cf. [44]. Indeed, assuming (here formally) G^0 Gâteaux differentiable and using (27) and the degree-1 homogeneity of R , we obtain the estimate for the directional derivative

$$[[G^0]'_q(t, q(t))](v) = \lim_{\varepsilon \rightarrow 0^+} \frac{G(t, q(t) + \varepsilon v) - G(t, q(t))}{\varepsilon} \geq -\frac{R(q(t) + \varepsilon v - q(t))}{\varepsilon} = -R(v).$$

Then, if $q(\cdot)$ would be smooth, we can differentiate (28) in t to obtain $\frac{d}{dt}G^0(t, q(t)) + R(\frac{d}{dt}q) = [G^0]'_t(t, q(t))$. Substituting $\frac{d}{dt}G^0(t, q(t)) = [G^0]'_t(t, q(t)) + [[G^0]'_q(t, q(t))](\frac{d}{dt}q)$ and subtracting it from the information we got from (27), we arrive at the *variational inequality*

$$[[G^0]'_q(t, q(t))](v - \frac{dq}{dt}) + R(v) \geq R(\frac{dq}{dt}) \quad (31)$$

to hold for any v . This is equivalent to the doubly-nonlinear evolution problem

$$\partial R(\frac{dq}{dt}) + [G^0]'_q(t, q(t)) \ni 0 \quad (32)$$

where ∂R denotes standardly the subdifferential of R . The right-hand side of (32) identifies the driving force $-[G^0]'_q(t, q(t))$ for the PTs. The inequality (31) just says that $\frac{d}{dt}q$ minimizes the functional $v \mapsto [[G^0]'_q(t, q(t))](v) + R(v)$, i.e. the sum of the power of elastic forces and the dissipation. This can be interpreted as a certain *minimum-type principle* for $\frac{d}{dt}q$ opposing the mentioned maximum-dissipation principle for $\frac{d}{dt}q$. It is related with the Levitas' *realizability principle* [38] (see also [48]) claiming that the PTs occur as soon as it is thermodynamically possible, namely

when the gain in energy through a particular PT is at least equal to the dissipated energy. In our case, G^0 is nonsmooth, however, and even involves the constraints $\lambda = \mathcal{L} \bullet \nu$ and $\nu \in \mathcal{G}^p(\Omega; \mathbb{R}^{3 \times 3})$ and the rigorous formulation and more detailed analysis of (32) is not obvious because $G^p(\Omega; \mathbb{R}^{3 \times 3})$ is not convex, and then Definition 5.1 helps substantially.

Under some qualification of the data $(\varphi, \mathcal{L}, |\cdot|_M, f, u_D, q_0, \rho)$, the existence of some energetic solution can be proved by a constructive way by approximation of the implicit Euler formula and the spacial finite-element-like discretization combined with laminated Young measures (4) and a penalization of the equality (15), which also suggest a numerical strategy. As already emphasized, the set $\mathcal{G}^p(\Omega; \mathbb{R}^{3 \times 3})$ cannot be explicitly implemented so we employ the smaller set $\mathcal{G}_{\text{lam}}^{p,k}(\Omega; \mathbb{R}^{3 \times 3})$ from (4), which, however, brings a necessity to treat the relation $\lambda = \mathcal{L} \bullet \nu$ with a “tolerance”, because, due to the compactness in λ 's caused by the regularizing nonlocal ρ -term in (24), it behaves like a constraint which, if treated without any tolerance, might destroy the convergence, cf. [63] or also [64, Prop.1.3.5].

To construct approximate solutions, we consider time steps $\tau > 0$, assuming that T/τ is integer and that $\tau \rightarrow 0$. Beside of this time discretization we will employ the finite-element method as space discretization. We assume that Ω is a polyhedral domain triangulated by simplicial triangulations, denoted by \mathcal{T}_h , where $h > 0$ is a mesh parameter satisfying $h \geq \max_{S \in \mathcal{T}_h} \text{diam}(S)$. We consider a countable set of h 's with $h \rightarrow 0$ which are nested, i.e. \mathcal{T}_{h_1} is a refinement of \mathcal{T}_{h_2} if $h_2 \geq h_1 > 0$.

We fix an order of lamination $\kappa \geq 0$ in (4); the concrete value of κ does not affect the theoretical convergence results but may, of course, substantially influence the rate of convergence and thus numerical results of concrete computational experiments if taken too small. We introduce the spatially discretized state space as

$$Q_h = \left\{ q = (u, \nu, \lambda) \in Q; \begin{array}{l} \nu \in \mathcal{G}_{\text{lam}}^{p,\kappa}(\Omega; \mathbb{R}^{3 \times 3}) \text{ and constant on each simplex of } \mathcal{T}_h, \\ \lambda \text{ constant on each simplex of } \mathcal{T}_h \end{array} \right\} \quad (33)$$

Note that each u with $(u, \nu, \lambda) \in Q_h$ is inevitably piecewise affine on \mathcal{T}_h , since ∇u is piecewise constant.

In addition to the two small parameters $\tau > 0$ and $h > 0$ we introduce a third small parameter $\varepsilon > 0$ which is used to relax the constraint $\lambda = \mathcal{L} \bullet \nu$. For this we introduce the relaxed, spatially discretized energy

$$G_h^\varepsilon(t, q) = \begin{cases} G(t, q) + \frac{1}{\varepsilon} \|\lambda - \mathcal{L} \bullet \nu\|^2 & \text{for } q \in Q_h, \\ +\infty & \text{for } q \in Q \setminus Q_h, \end{cases} \quad (34)$$

where $\mathcal{L} \bullet \nu$ is from (23) and where $\|\cdot\|$ is the norm in a space to which $L^\infty(\Omega; \mathbb{R}^{1+M}) + W^{\alpha,r}(\Omega; \mathbb{R}^{1+M})$ is embedded compactly, e.g. the space $H^{-1}(\Omega; \mathbb{R}^{1+M}) := W_0^{1,2}(\Omega; \mathbb{R}^{1+M})^*$; recall that L^∞ stands, as standard, for the space of measurable essentially bounded functions.

With these definitions, we consider a fully implicit algorithm based on the following incremental problem: Let $q_\tau^0 = q_0$ be a given initial condition, and, for $k = 1, \dots, T/\tau$ we define $(q_{\tau,h}^{\varepsilon,k})_{k=1, \dots, T/\tau}$ to be a solution of the minimization problems

$$\left. \begin{array}{l} \text{Minimize } G_h^\varepsilon(k\tau, q) + R(q - q^{k-1}) \\ \text{subject to } q = (u, \nu, \lambda) \in Q_h. \end{array} \right\} \quad (35)$$

For $k = 0$, we naturally put $q_{\tau,h}^{\varepsilon,k} = q_0$, a given initial condition. As R involves only λ , the component λ_0 of $q_0 = (u_0, \nu_0, \lambda_0)$ is what plays role. In general, to ensure the energy estimate (42) below, the initial condition must be stable; here, for simplicity, in (37) we will assume even more special q_0 used in Section 6. The stability is most easily expressed via the *sets of stable states*

$$\mathcal{S}_h^\varepsilon(t) := \{q \in Q; G_h^\varepsilon(t, q) < +\infty, \forall \tilde{q} \in Q : G_h^\varepsilon(t, q) \leq G_h^\varepsilon(t, \tilde{q}) + R(\tilde{q} - q)\}. \quad (36)$$

The stability condition (27) then means $q(t) \in \mathcal{S}_h^\varepsilon(t)$ for all $t \in [0, T]$. The condition (37c,d) below will guarantee $q_0 \in \mathcal{S}_h^\varepsilon(0)$. Also, for simplicity, assume u_D constant in time and, again in agreement with Section 6, even zero; cf. Remark 5.9 for a generalization.

Let us denote by $q_{\tau,h}^\varepsilon$ the piecewise constant approximate solution, i.e. $q_{\tau,h}^\varepsilon(t) := q_{\tau,h}^{\varepsilon,k}$ for $(k-1)\tau < t \leq k\tau$, $k = 0, \dots, T/\tau$. Beside the standard notation for $W^{\alpha,p}$ - and L^p -spaces already explained, we now use also ‘‘BV’’ for the space of functions with bounded variations. The numerical stability of the proposed scheme is based on the following a-priori estimates.

Proposition 5.5 *Let, for $\kappa \geq 0$ fixed,*

$$f \in W^{1,1}(0, T; W^{1/p-1, p/(p-1)}(\Gamma_N; \mathbb{R}^3)), \quad u_D = 0, \quad (37a)$$

$$\varepsilon|A|^p - C \leq \varphi(A) \leq C(1 + |A|^p) \quad \text{for some } \varepsilon > 0, C < +\infty, \quad (37b)$$

$$f(0, \cdot) = 0 \quad \text{and} \quad q_0 = (u_0, \nu_0, \lambda_0) \in Q^0 \quad \text{with} \quad (37c)$$

$$u_0 = 0, \quad \nu_0 \in \mathcal{G}_{\text{lam}}^{p,\kappa}(\Omega; \mathbb{R}^{3 \times 3}) \quad \text{spatially constant and minimizing } \varphi. \quad (37d)$$

Then the following a-priori estimates for $q_{\tau,h}^\varepsilon = (u_{\tau,h}^\varepsilon, \nu_{\tau,h}^\varepsilon, \lambda_{\tau,h}^\varepsilon) : [0, T] \rightarrow Q_h$ hold:

$$\|u_{\tau,h}^\varepsilon\|_{L^\infty(0, T; W^{1,p}(\Omega; \mathbb{R}^3))} \leq C_0, \quad (38)$$

$$\|\lambda_{\tau,h}^\varepsilon\|_{\text{BV}(0, T; L^1(\Omega; \mathbb{R}^{1+M})) \cap L^\infty(0, T; L^\infty(\Omega; \mathbb{R}^{1+M})) \cap W^{\alpha, r}(\Omega; \mathbb{R}^{1+M})} \leq C_1, \quad (39)$$

$$\|\mathfrak{G}_{\tau,h}^\varepsilon\|_{\text{BV}(0, T)} \leq C_2 \quad \text{with } \mathfrak{G}_{\tau,h}^\varepsilon(t) := G_h^\varepsilon(k\tau, q_{\tau,h}^{\varepsilon,k}) \text{ for } t \in ((k-1)\tau, k\tau]. \quad (40)$$

Moreover, $q_{\tau,h}^\varepsilon$ is stable in the following sense

$$\forall \tilde{q} \in Q_h : \mathfrak{G}_{\tau,h}^\varepsilon(k\tau) = G_h^\varepsilon(k\tau, q_{\tau,h}^\varepsilon(k\tau)) \leq G_h^\varepsilon(k\tau, \tilde{q}) + R(q_{\tau,h}^\varepsilon(k\tau) - \tilde{q}) \quad (41)$$

for all $k = 0, 1, \dots, T/\tau$ and satisfies the two-sided discrete energy inequality

$$\begin{aligned} \int_0^t \int_{\Gamma_N} \frac{\partial f(s, x)}{\partial s} \cdot u_{\tau,h}^\varepsilon(s, x) \, dx ds &\leq \mathfrak{G}_{\tau,h}^\varepsilon(t) + \text{Var}_R(q_{\tau,h}^\varepsilon; 0, t) - \mathfrak{G}_{\tau,h}^\varepsilon(0) \\ &\leq \int_0^t \int_{\Gamma_N} \frac{\partial f(s, x)}{\partial s} \cdot u_{\tau,h}^\varepsilon(s - \tau, x) \, dx ds \end{aligned} \quad (42)$$

for $t = \tau k$, $k = 0, 1, \dots, T/\tau$.

Sketch of the proof of Proposition 5.5. The discrete stability condition (41) follows by using successively that $q_{\tau,h}^{\varepsilon,k}$ is a solution to (35) and the triangle inequality (18) for R :

$$\begin{aligned} G_h^\varepsilon(k\tau, q_{\tau,h}^{\varepsilon,k}) &\leq G_h^\varepsilon(k\tau, \tilde{q}) + R(\tilde{q} - q_{\tau,h}^{\varepsilon,k-1}) - R(q_{\tau,h}^{\varepsilon,k} - q_{\tau,h}^{\varepsilon,k-1}) \\ &\leq G_h^\varepsilon(k\tau, \tilde{q}) + R(\tilde{q} - q_{\tau,h}^{\varepsilon,k}) \end{aligned} \quad (43)$$

for any $k = 1, \dots, K = T/\tau$.

As to (42), we again use that $q_{\tau,h}^{\varepsilon,k}$ solves (35) and, comparing it with $q_{\tau,h}^{\varepsilon,k-1}$, we get

$$\begin{aligned} & G_h^\varepsilon(k\tau, q_{\tau,h}^{\varepsilon,k}) - G_h^\varepsilon((k-1)\tau, q_{\tau,h}^{\varepsilon,k-1}) + R(q_{\tau,h}^{\varepsilon,k} - q_{\tau,h}^{\varepsilon,k-1}) \\ & \leq G_h^\varepsilon(k\tau, q_{\tau,h}^{\varepsilon,k-1}) - G_h^\varepsilon((k-1)\tau, q_{\tau,h}^{\varepsilon,k-1}) \\ & = \int_{(k-1)\tau}^{k\tau} \frac{\partial G_h^\varepsilon(t, q_{\tau,h}^{\varepsilon,k-1})}{\partial t} dt = \int_{(k-1)\tau}^{k\tau} \int_{\Gamma_N} \frac{\partial f(t, x)}{\partial t} \cdot u_{\tau,h}^\varepsilon(t - \tau, x) dx dt \end{aligned} \quad (44)$$

and then the second estimate in (42) after a summation. As to the first estimate in (42), by the stability (43) written for $q_{\tau,h}^{\varepsilon,k-1}$, we can see that $q_{\tau,h}^{\varepsilon,k-1}$ minimizes the functional $q \mapsto G_h^\varepsilon((k-1)\tau, q) + R(q - q_{\tau,h}^{\varepsilon,k-1})$, and therefore, by inserting $q = q_{\tau,h}^{\varepsilon,k}$, we find

$$\begin{aligned} & G_h^\varepsilon(k\tau, q_{\tau,h}^{\varepsilon,k}) - G_h^\varepsilon((k-1)\tau, q_{\tau,h}^{\varepsilon,k-1}) + R(q_{\tau,h}^{\varepsilon,k} - q_{\tau,h}^{\varepsilon,k-1}) \\ & \geq G_h^\varepsilon(k\tau, q_{\tau,h}^{\varepsilon,k}) - G_h^\varepsilon((k-1)\tau, q_{\tau,h}^{\varepsilon,k}) \end{aligned} \quad (45)$$

$$= \int_{(k-1)\tau}^{k\tau} \frac{\partial G_h^\varepsilon(t, q_{\tau,h}^{\varepsilon,k})}{\partial t} dt = \int_{(k-1)\tau}^{k\tau} \int_{\Gamma_N} \frac{\partial f(t, x)}{\partial t} \cdot u_{\tau,h}^\varepsilon(t, x) dx dt. \quad (46)$$

By a summation we obtain the first part of (42). Note that, for $k = 1$, we used the stability of $q_{\tau,h}^{\varepsilon,0} = q_0$, i.e.

$$\forall \tilde{q} \in Q_h : \quad G_h^\varepsilon(0, q_0) \leq G_h^\varepsilon(0, \tilde{q}) + R(\lambda_0 - \tilde{\lambda}), \quad (47)$$

which is assumed in (37c,d).

The BV-bound in the estimate (39) then follows directly from (44), while the L^∞ -bound is obvious since $\lambda_{\tau,h}^\varepsilon(t, x) \in \Delta$ for a.a. $(t, x) \in [0, T] \times \Omega$ and $\Delta \subset \mathbb{R}^{1+M}$ is bounded, and eventually by summing (44) for $k = 1, \dots, T/\tau$, we get $G_{\tau,h}^\varepsilon(t, q_{\tau,h}^\varepsilon(t))$ bounded from above uniformly in $t \in [0, T]$ so that, in view of the coercivity (37b) and of $\rho > 0$ in (24), the bounds for $\|u_{\tau,h}^\varepsilon(t)\|_{W^{1,p}(\Omega; \mathbb{R}^3)}$ and for $|\lambda_{\tau,h}^\varepsilon(t)|_{\alpha,r}$ uniform in $t \in [0, T]$ follow by using also (37a) and the discrete Gronwall inequality; note that not k but $k-1$ level occurs on the right-hand side of (44) so no restriction on τ is needed. By (44) and (46) and also by using (38)–(39), it holds

$$\begin{aligned} \text{Var}(\mathfrak{G}_{\tau,h}^\varepsilon; 0, T) &= \sum_{k=1}^{T/\tau} |G_h^\varepsilon(k\tau, q_{\tau,h}^{\varepsilon,k}) - G_h^\varepsilon((k-1)\tau, q_{\tau,h}^{\varepsilon,k-1})| \\ &\leq \sum_{k=1}^{T/\tau} \max \left(\int_{(k-1)\tau}^{k\tau} \left| \frac{\partial G_h^\varepsilon(t, q_{\tau,h}^{\varepsilon,k-1})}{\partial t} \right| dt, R(q_{\tau,h}^{\varepsilon,k} - q_{\tau,h}^{\varepsilon,k-1}) + \int_{(k-1)\tau}^{k\tau} \left| \frac{\partial G_h^\varepsilon(t, q_{\tau,h}^{\varepsilon,k})}{\partial t} \right| dt \right) \\ &\leq \text{Var}_R(q_{\tau,h}^\varepsilon; 0, T) + \|u|_{\Gamma_N}\|_{L^\infty(\Omega; W^{1-1/p,p}(\Gamma_N; \mathbb{R}^3))} \left\| \frac{\partial f}{\partial t} \right\|_{L^1(0,T; W^{1/p-1,p/(p-1)}(\Gamma_N; \mathbb{R}^3))} \end{aligned} \quad (48)$$

proving a bound for $\|\mathfrak{G}_{\tau,h}^\varepsilon\|_{\text{BV}(0,T)} := \int_0^T |\mathfrak{G}_{\tau,h}^\varepsilon| dt + \text{Var}(\mathfrak{G}_{\tau,h}^\varepsilon; 0, T)$, i.e. (40). \square

Now we are ready to state the convergence for $(\tau, h, \varepsilon) \rightarrow (0, 0, 0)$ of the proposed scheme. Under some rather strong “nonbuckling” conditions it was shown in a weak form in [36, 68].

The major condition for treating the limit is that G_h^ε converges in the sense of Γ -convergence to towards the limit energy G^0 , where now all energies are assumed to be defined on Q , but are allowed to take the value $+\infty$. First we specify the sense in which the convergence of sequences is taken:

$$q_j = (u_j, \nu_j, \lambda_j) \xrightarrow{*} q = (u, \nu, \lambda) \text{ in } Q \iff \begin{cases} u_j \rightharpoonup u & \text{in } W^{1,p}(\Omega, \mathbb{R}^3), \\ \nu_j \xrightarrow{*} \nu & \text{in } \mathcal{G}^p(\Omega, \mathbb{R}^{3 \times 3}), \\ \lambda_j \rightharpoonup \lambda & \text{in } W^{\alpha,r}(\Omega, \mathbb{R}^{1+M}), \end{cases} \quad (49)$$

where the weak* convergence $\nu_j \xrightarrow{*} \nu$ means that

$$\forall h \in L^1(\Omega; C_0(\mathbb{R}^{3 \times 3})) : \lim_{j \rightarrow \infty} \int_{\Omega} \int_{\mathbb{R}^{3 \times 3}} h(x, A) [\nu_j]_x(dA) dx = \int_{\Omega} \int_{\mathbb{R}^{3 \times 3}} h(x, A) \nu_x(dA) dx.$$

We consider this as the major convergence in our extended state space Q . First we note that the dissipation functional R , which is independent of τ, h , and ε , is weakly continuous, namely

$$q_j \xrightarrow{*} q \text{ and } \tilde{q}_j \xrightarrow{*} \tilde{q} \text{ in } Q \implies R(q_j - \tilde{q}_j) \rightarrow R(q - \tilde{q}). \quad (50)$$

Moreover, we need the collection of triangulations $\{\mathcal{T}_h\}_{h>0}$ to be *regular*, i.e. there is $c > 0$ such that, for every finite element $E \in \mathcal{T}_h$, $r_E/\ell_E > c$ for any $h > 0$ where ℓ_E is the length of the longest edge (side) and r_E is the radius of the largest ball inscribed into E .

The part (i) in the following proposition is a condition on *uniform compactness* or *uniform coercivity* with respect to the sequential weak* topology of Q . The parts (ii) and (iii) state exactly that $G^0(t, \cdot)$ is the so-called Γ -limit of the family $\{G_h^\varepsilon(t, \cdot)\}$ conditioned by a certain *numerical-stability criterion* $h \leq H(\varepsilon)$.

Proposition 5.6 *Let (37) hold and let $\{\mathcal{T}_h\}_{h>0}$ be regular. For each $t \in [0, T]$ we have the following three properties:*

(i) (**Uniform compactness.**) *If the family $\{q_h^\varepsilon\}_{\varepsilon, h>0}$ and $t_\tau \in [0, T]$ satisfy*

$$\forall \varepsilon, h > 0 : \quad G_h^\varepsilon(t_\tau, q_h^\varepsilon) \leq E_0 < +\infty \quad (51)$$

then there exists a subsequence $\{q_{h_k}^{\varepsilon_k}\}_{k \in \mathbb{N}}$ and $q \in Q$, such that $q_{h_k}^{\varepsilon_k} \xrightarrow{} q$ in Q .*

(ii) (**Relaxation.**) *For each family $(q_h^\varepsilon)_{\varepsilon, h}$ in Q with $q_h^\varepsilon \xrightarrow{*} q$ we have*

$$\liminf_{(t_\tau, h, \varepsilon) \rightarrow (t, 0, 0)} G_h^\varepsilon(t_\tau, q_h^\varepsilon) \geq G^0(t, q). \quad (52)$$

(iii) (**Recovery sequence.**) *If (51) holds, then there is $H : \mathbb{R}^+ \rightarrow \mathbb{R}^+$ (depending on E_0 from (51)) such that for all $q \in Q$ there exists a family $(q_h^\varepsilon)_{\varepsilon, h}$ with $q_h^\varepsilon \in Q_h$ such that*

$$q_h^\varepsilon \xrightarrow{*} q \quad \text{and} \quad \lim_{\substack{h \leq H(\varepsilon) \\ (t_\tau, h, \varepsilon) \rightarrow (t, 0, 0)}} G_h^\varepsilon(t_\tau, q_h^\varepsilon) = G^0(t, q). \quad (53)$$

Sketch of the proof. Ad (i): Using the assumption (37a,b) together with (51), we obtain the standard coercivity properties implying for $q_h^\varepsilon = (u_h^\varepsilon, \nu_h^\varepsilon, \lambda_h^\varepsilon)$ with $G_h^\varepsilon(t, q_h^\varepsilon) \leq E_0$ the bounds

$$\|u_h^\varepsilon\|_{W^{1,p}(\Omega; \mathbb{R}^3)} + \int_{\Omega} \int_{\mathbb{R}^{3 \times 3}} (1+|A|^p)(\nu_h^\varepsilon)_x(dA)dx + \|\lambda_h^\varepsilon\|_{W^{\alpha,r}(\Omega; \mathbb{R}^{1+M})} \leq C_0, \quad (54)$$

where C_0 depends only on E_0 . From this, the existence of a weak* convergent subsequence follows by standard arguments.

Ad (ii): We may assume that $\liminf_{(t_\tau, h, \varepsilon) \rightarrow (t, 0, 0)} G_h^\varepsilon(t_\tau, q_h^\varepsilon) =: \gamma < \infty$, since otherwise there is nothing to be shown. By our assumptions $G(t, q) \geq -C_G$ and thus, we conclude $\|\lambda_h^\varepsilon - \mathcal{L} \bullet \nu_h^\varepsilon\| \leq (\gamma + C_G + 1)\varepsilon$ for (t_τ, h, ε) sufficiently close to $(t, 0, 0)$. Hence, $q_h^\varepsilon \xrightarrow{*} q = (u, \nu, \lambda)$ implies $\lambda = \mathcal{L} \bullet \nu$, which means $q \in Q^0$. Moreover, the definition of the convergence $q_h^\varepsilon \xrightarrow{*} q$ implies $G(t_\tau, q_h^\varepsilon) \rightarrow G(t, q)$, where we essentially use the property of the gradient Young measures in $\mathcal{G}^p(\Omega; \mathbb{R}^{3 \times 3})$ and the assumption (37a) which ensures $f(t_\tau) \rightarrow f(t)$ in $W^{1/p-1, p/(p-1)}(\Gamma_N; \mathbb{R}^3)$ while we also have $u_h^\varepsilon \rightharpoonup u$ in $W^{1-1/p, p}(\Gamma_N; \mathbb{R}^3)$ so that $\int_{\Gamma_N} f(t_\tau, x) \cdot u_h^\varepsilon(x) dx \rightarrow \int_{\Gamma_N} f(t, x) \cdot u(x) dx$, and eventually $\lambda_h^\varepsilon \rightharpoonup \lambda$ in $W^{\alpha, r}(\Omega; \mathbb{R}^{1+M})$ implies $\liminf_{(h, \varepsilon) \rightarrow (0, 0)} |\lambda_h^\varepsilon|_{\alpha, r}^r \geq |\lambda|_{\alpha, r}^r$. Because of $q \in Q^0$ we thus have

$$\begin{aligned} G^0(t, q) = G(t, q) &\leq \lim_{(t_\tau, h, \varepsilon) \rightarrow (t, 0, 0)} (G(t_\tau, q_h^\varepsilon) - |\lambda_h^\varepsilon|_{\alpha, r}^r) \\ &\quad + \liminf_{(h, \varepsilon) \rightarrow (0, 0)} |\lambda_h^\varepsilon|_{\alpha, r}^r \leq \liminf_{(t_\tau, h, \varepsilon) \rightarrow (t, 0, 0)} G_h^\varepsilon(t_\tau, q_h^\varepsilon), \end{aligned} \quad (55)$$

which is the desired lower estimate of the possible limits.

Ad (iii): First consider the case $q \notin Q^0$, which leads to $G^0(t, q) = \infty$. Now every sequence with $q_h^\varepsilon \xrightarrow{*} q$ is a recovery sequence. We have $\lambda_h^\varepsilon - \mathcal{L} \bullet \nu_h^\varepsilon \xrightarrow{*} \lambda - \mathcal{L} \bullet \nu =: g$ and $q \notin Q^0$ implies $g \neq 0$. Thus, by lower semicontinuity of the norm we conclude

$$\liminf_{(h, \varepsilon) \rightarrow (0, 0)} \|\lambda_h^\varepsilon - \mathcal{L} \bullet \nu_h^\varepsilon\| \geq \|g\| > 0. \quad (56)$$

From this we easily obtain $\liminf_{(h, \varepsilon) \rightarrow (0, 0)} G_h^\varepsilon(t, q_h^\varepsilon) = \infty = G^0(t, q)$, as desired.

Next, we consider the case $q \in Q^0$. By the definition of $\mathcal{G}^p(\Omega; \mathbb{R}^{3 \times 3})$, there is a $W^{1,p}$ -bounded sequence $\{u_k\}_{k \in \mathbb{N}}$ whose gradients attains ν , i.e.

$$\forall h \in L^1(\Omega; C_0(\mathbb{R}^{3 \times 3})) : \lim_{k \rightarrow \infty} \int_{\Omega} h(x, \nabla u_k) dx = \int_{\Omega} \int_{\mathbb{R}^{3 \times 3}} h(x, A) \nu_x(dA) dx. \quad (57)$$

Using the assumed regularity of the triangulations, we can further approximate each u_k by element-wise affine functions and as well as of $W^{\alpha, r}$ -functions by element-wise constant functions. Taking a suitable diagonal sequence, this yields a sequence $\{q_h\}_{h>0}$, $q_h \in Q_h$, converging weakly* to q and thus shows that $\bigcup_{h>0} Q_h$ is weakly* dense in Q .

Using the compactness proved at the point (i) and the separability of the spaces of the test functions for the weak* convergence (49), we can think about a metric, say ϱ , inducing this convergence on the compact set in question. Restricted our consideration on that compact set, we can consider Q^0 a closed (hence compact) subset of Q . Due to the density of $\bigcup_{h>0} Q_h$ in Q , for some sufficiently small $h_\delta > 0$,

for any $q \in Q^0$ there is $\tilde{q} \in Q_h$, $\varrho(q, \tilde{q}) \leq \delta$; the proof is by a contradiction: if for any $h > 0$ there would be some $q_h \in Q^0$ whose δ -neighbourhood would be disjoint with Q_h , by compactness of Q^0 we would get a limit q of a subsequence of $\{q_h\}$ converging for $h \rightarrow 0$ whose $\delta/2$ -neighbourhood would still be disjoint with $\bigcup_{h>0} Q_h$.

As the norm $\|\cdot\|$ in (34) is weakly* continuous on $W^{\alpha,r}(\Omega; \mathbb{R}^{1+M})$ as well as on $L^\infty(\Omega; \mathbb{R}^{1+M})$ and $L : q = (u, \nu, \lambda) \mapsto \lambda - \mathcal{L} \bullet \nu$ is weakly* continuous on Q to $W^{\alpha,r}(\Omega; \mathbb{R}^{1+M}) + L^\infty(\Omega; \mathbb{R}^{1+M})$, hence continuous with respect to the metric ϱ , for any $\varepsilon > 0$ there is $\delta > 0$ such that $\varrho(q, \tilde{q}) \leq \delta$ implies $\|L(q - \tilde{q})\| \leq \varepsilon$.

Linking those two results, we can see that for any $\varepsilon > 0$ there is $H(\varepsilon) > 0$ sufficiently small, namely $H(\varepsilon) = h_\delta$, such that for any $h \leq H(\varepsilon)$ and for any $q \in Q_0$ there is $\tilde{q} \in Q_h$ such that $\varepsilon \geq \|L(q - \tilde{q})\| = \|L\tilde{q}\| = \|\tilde{\lambda} - \mathcal{L} \bullet \tilde{\nu}\|$. Then we put $q_h^\varepsilon = \tilde{q}$. Note that $\frac{1}{\varepsilon} \|\lambda_h^\varepsilon - \mathcal{L} \bullet \nu_h^\varepsilon\|^2 \leq \frac{1}{\varepsilon} \varepsilon^2 = \varepsilon \rightarrow 0$. \square

Further important properties of the underlying system are the weak* closeness of the stable states and the continuity of the energy when restricted to the stable sets. The first property follows easily since the dissipation is continuous. As the energies G_h^ε Γ -converge to G^0 we already have the lower semicontinuity (52). The second property (58) reflects the fact that stable states are already energetically favorable states. Hence, these states do not contain unnecessary oscillations which could lead to a drop of the energy in the limit $(t_\tau, \varepsilon, h) \rightarrow 0$.

Proposition 5.7 *Let (51) hold and $(t_\tau, h, \varepsilon) \rightarrow (t_*, 0, 0)$ with $h \leq H(\varepsilon)$, let $q_h^\varepsilon \in \mathcal{S}_h^\varepsilon(t_\tau)$ with $\mathcal{S}_h^\varepsilon(t_\tau)$ from (36), and let $q_h^\varepsilon \xrightarrow{*} q_*$, then we have*

$$q_* \in \mathcal{S}^0(t_*) \quad \text{and} \quad \lim_{\substack{h \leq H(\varepsilon) \\ (t_\tau, h, \varepsilon) \rightarrow (t_*, 0, 0)}} G_h^\varepsilon(t_\tau, q_h^\varepsilon) = G^0(t_*, q_*) \quad (58)$$

with \mathcal{S}^0 from (30) and with the stability criterion $h \leq H(\varepsilon)$ from Proposition 5.6(iii).

Proof: For the stability result $q_* \in \mathcal{S}^0(t_*)$ we have to prove stability with respect to every test state $\tilde{q} \in Q$. As (51) is assumed, Proposition 5.6(iii) says that, for each such state, there exists a recovery sequence \tilde{q}_h^ε with $\tilde{q}_h^\varepsilon \xrightarrow{*} \tilde{q}$ and $\lim_{(t_\tau, h, \varepsilon) \rightarrow (t_*, 0, 0), h \leq H(\varepsilon)} G_h^\varepsilon(t_\tau, \tilde{q}_h^\varepsilon) = G^0(t_*, \tilde{q})$. Now the stability of q_h^ε gives

$$G_h^\varepsilon(t_\tau, q_h^\varepsilon) \leq G_h^\varepsilon(t_\tau, \tilde{q}_h^\varepsilon) + R(\tilde{q}_h^\varepsilon - q_h^\varepsilon). \quad (59)$$

On the right-hand side we can pass to the limit using the recovery properties and the weak continuity of R , cf. (50). On the left-hand side we take the \liminf and use Proposition 5.6(iii). Thus, we obtain

$$\begin{aligned} G^0(t_*, q_*) &\leq \liminf_{(t_\tau, h, \varepsilon) \rightarrow (t_*, 0, 0)} G_h^\varepsilon(t_\tau, q_h^\varepsilon) \\ &\leq \lim_{\substack{h \leq H(\varepsilon) \\ (t_\tau, h, \varepsilon) \rightarrow (t_*, 0, 0)}} G_h^\varepsilon(t_\tau, \tilde{q}_h^\varepsilon) + R(\tilde{q}_h^\varepsilon - q_h^\varepsilon) = G^0(t_*, \tilde{q}) + R(\tilde{q} - q_*), \end{aligned} \quad (60)$$

which is the desired stability. The convergence of the energy follows by choosing $\tilde{q} = q_*$ in (60). \square

Our final result of the states the convergence of the numerical scheme, the implementation of which will be discussed in the next section. As we have no uniqueness of the solutions we cannot expect that the whole sequence of our approximations will

converge. We will show that choosing a suitably converging subsequence we obtain a limit which is an energetic solution, i.e., it satisfies the stability condition (27) and the energy balance (28). In fact, any such limit point obtained from our numerical scheme is automatically a solution. However, we are not able to provide convergence rates since the problem does not have any kind of convexity and smoothness properties, which are usually available in well-posed problems of continuum mechanics.

Theorem 5.8 *Let (37) hold and let $\{q_{\tau,h}^\varepsilon\}_{(\tau,h,\varepsilon)}$ be a family of approximations constructed as above such that $(\tau, h, \varepsilon) \rightarrow 0$, such that*

$$q_{\tau,h}^\varepsilon(0) \in \mathcal{S}_h^\varepsilon(0), \quad q_{\tau,h}^\varepsilon(0) \xrightarrow{*} q_0, \quad \text{and} \quad G_h^\varepsilon(0, q_{\tau,h}^\varepsilon(0)) \rightarrow G^0(0, q_0). \quad (61)$$

Then, there exists a subsequence $\{(\tau_k, h_k, \varepsilon_k)\}_{k \in \mathbb{N}}$ with $(\tau_k, h_k, \varepsilon_k) \rightarrow (0, 0, 0)$ for $k \rightarrow \infty$ satisfying the stability criterion $h_k \leq H(\varepsilon_k)$ from Proposition 5.6(iii) and a limit process $q : [0, T] \rightarrow Q$ with $q(0) = q_0$, such that the following holds. (We shortly write $q_k = (u_k, \nu_k, \lambda_k)$ for $q_{\tau_k, h_k}^{\varepsilon_k} = (u_{\tau_k, h_k}^{\varepsilon_k}, \nu_{\tau_k, h_k}^{\varepsilon_k}, \lambda_{\tau_k, h_k}^{\varepsilon_k})$.)

- (i) *$q : [0, T] \rightarrow Q^0 \subset Q$ is an energetic solution, i.e., q satisfies (27) and (28), and also it holds $\lambda \in L^\infty([0, T]; W^{\alpha, r}(\Omega; \mathbb{R}^{1+M})) \cap \text{BV}([0, T], L^1(\Omega; \mathbb{R}^{1+M}))$ and $u : [0, T] \rightarrow W^{1, p}(\Omega; \mathbb{R}^3)$ is bounded.*
- (ii) *For all $t \in [0, T]$ we have $\lambda_k(t) \rightharpoonup \lambda(t)$ in $W^{\alpha, r}(\Omega; \mathbb{R}^{1+M})$.*
- (iii) *For all $t \in [0, T]$ we have $\text{Var}_R(q_k; 0, t) \rightarrow \text{Var}_R(q; 0, t)$.*
- (iv) *For all $t \in [0, T]$ we have $G_{h_k}^{\varepsilon_k}(t, q_k(t)) \rightarrow G^0(t, q(t))$.*
- (v) *$\frac{\partial}{\partial t} G_{h_k}^{\varepsilon_k}(\cdot, q_k(\cdot)) \xrightarrow{*} \frac{\partial}{\partial t} G^0(\cdot, q(\cdot))$ in $L^\infty(0, T)$.*
- (vi) *For all $t \in [0, T]$ there is a subsequence $\{k_l\}_{l \in \mathbb{N}}$ such that $q_{k_l}(t) \xrightarrow{*} q(t)$ in Q .*

In fact, (61) is satisfied automatically if (37c,d) is assumed. We pronounced (61) here for its more general character.

Sketch of proof of Theorem 5.8. Our sketch follows the six steps for the existence proof formulated in [20, 44].

Step 1: A priori estimates. This part is exactly the content of Proposition 5.5, which provides uniform bounds for $q_{\tau,h}^\varepsilon : [0, T] \rightarrow Q$. In particular, (40) makes (51) hold and we have the results from Propositions 5.6 and 5.7 at our disposal.

Step 2: Selection of subsequences. Since the $\lambda_{\tau,h}^\varepsilon : [0, T] \times \Omega \rightarrow \mathbb{R}^{1+M}$ is uniformly bounded in $\text{BV}([0, T]; L^1(\Omega; \mathbb{R}^{1+M})) \cap L^\infty([0, T]; W^{\alpha, r}(\Omega; \mathbb{R}^{1+M}))$ and since the scalar functions $\mathfrak{G}_{\tau,h}^\varepsilon : [0, T] \rightarrow \mathbb{R}$ and $\mathfrak{D}_{\tau,h}^\varepsilon : t \mapsto \text{Var}_R(q_{\tau,h}^\varepsilon; 0, t)$ are uniformly bounded in $\text{BV}([0, T])$, we may apply Helly's selection principle to find a subsequence $\{(\tau_k, h_k, \varepsilon_k)\}_{k \in \mathbb{N}}$ such that for all $t \in [0, T]$ we have the following convergence:

$$\lambda_{\tau_k, h_k}^{\varepsilon_k}(t) \rightharpoonup \lambda(t) \text{ in } W^{\alpha, r}(\Omega; \mathbb{R}^{1+M}), \quad \mathfrak{G}_{\tau_k, h_k}^{\varepsilon_k}(t) \rightarrow \mathfrak{G}(t), \quad \mathfrak{D}_{\tau_k, h_k}^{\varepsilon_k}(t) \rightarrow \mathfrak{D}(t),$$

for suitable limit functions λ , \mathfrak{G} and \mathfrak{D} , which lie in the corresponding spaces and satisfy the same bounds as the corresponding sequences. For the λ -component one has to use the Banach-space valued version of Helly's selection principle, see [41, 44].

This shows that the convergence properties at the point (ii) hold. We further set

$$\mathfrak{F}_k(t) = \frac{\partial}{\partial t} \mathfrak{G}_{\tau_k, h_k}^{\varepsilon_k}(t, q_k(t)) \quad (62)$$

to denote the power of the external forces. Choosing another subsequence (not relabeled), if necessary, we also obtain

$$\mathfrak{P}_k \xrightarrow{*} \mathfrak{p} \text{ in } L^\infty([0, T]), \quad (63)$$

since closed balls in $L^\infty([0, T])$ are sequentially weakly* compact.

To define the limit function $q(t) \in Q$, we still need to specify the components u and ν . For this, we treat now each $t \in [0, T]$ separately. Note that the coupling between different time levels occurs only via the component λ , which is already controlled.

For fixed t , we choose (a t -dependent) subsequence $\{q_{K_l^t}(t)\}_{l \in \mathbb{N}}$ of $\{q_k(t)\}_{k \in \mathbb{N}}$ such that, for $l \rightarrow \infty$, we have

$$\mathfrak{P}_{K_l^t}(t) \rightarrow \mathfrak{P}(t) := \limsup_{k \rightarrow \infty} \mathfrak{P}_k(t) \quad \text{and} \quad q_{K_l^t}(t) \xrightarrow{*} q(t). \quad (64)$$

The choice of the subsequence is first made such the condition for \mathfrak{P} holds. Afterwards, we choose a further subsequence (not relabeled) to make $q_{K_l^t}(t)$ convergence. Here we again use the a priori bounds of Step 1. Thus, the limiting process $q : [0, T] \rightarrow Q$ is defined now.

From $\mathfrak{P}_k(t) = \int_{\Gamma_N} \frac{\partial}{\partial t} f(t, x) \cdot u_k(t, x) dx$ we easily conclude that $\mathfrak{P}(t) = \frac{\partial}{\partial t} G^0(t, q(t))$. Using Fatou's lemma we conclude $\mathfrak{p}(t) \leq \mathfrak{P}(t)$.

Step 3: Stability of the limit process. The stability of the limit process q is now a direct consequence of Proposition 5.7. For fixed $t \in [0, T]$ consider the sequence $\{q_{K_l^t}(t)\}_{l \in \mathbb{N}}$, which consists of piecewise constant functions. Hence, we have $q_{K_l^t}(t) = q_{K_l^t}(\hat{t}_l)$ with $\hat{t}_l = \max\{\kappa \tau_{K_l^t} \leq t; \kappa \in \mathbb{N} \cup \{0\}\}$ and, by Proposition 5.5, $q_{K_l^t}(\hat{t}_l) \in \mathcal{S}(\hat{t}_l)$. Since $\hat{t}_l \rightarrow t$, we conclude $q(t) \in \mathcal{S}(t)$ as desired.

Step 4: Upper energy estimate. By the convergence properties established above, we immediately see that the two-sided energy estimate (42) leads to the identity

$$\int_0^t \mathfrak{p}(s) ds \leq \mathfrak{G}(t) + \mathfrak{D}(t) - \mathfrak{G}(0) \leq \int_0^t \mathfrak{p}(s) ds \leq \int_0^t \mathfrak{P}(s) ds. \quad (65)$$

Note that the time shift in the right-hand side in (42) has no effect in the limit $t_k \rightarrow 0$, as $\frac{\partial}{\partial t} f(t, \cdot)$ is continuous in $t \in [0, T]$.

Now we use that the family $G_{\tau, h}^\varepsilon$ has the Γ -limit G^0 , hence we conclude $G^0(t, q(t)) \leq \lim_{l \rightarrow \infty} \mathfrak{G}_{K_l^t}(t, q_{K_l^t}(t)) = \mathfrak{G}(t)$. Moreover, by (61) we have $\mathfrak{G}(0) = G^0(0, q(0))$. Similarly, we have $\text{Var}_R(q; 0, t) \leq \mathfrak{D}(t)$. Inserting this into (65) we obtain

$$\begin{aligned} G^0(t, q(t)) + \text{Var}_R(q; 0, t) - G^0(0, q(0)) &\leq \mathfrak{G}(t) + \mathfrak{D}(t) - \mathfrak{G}(0) \\ &\leq \int_0^t \mathfrak{P}(s) ds = \int_0^t \frac{\partial}{\partial s} G^0(s, q(s)) ds, \end{aligned} \quad (66)$$

which is the desired upper energy estimate.

Step 5: Lower energy estimate. The opposite estimate $G^0(t, q(t)) + \text{Var}_R(q; 0, t) - G^0(0, q(0)) \geq \int_0^t \frac{\partial}{\partial s} G^0(s, q(s)) ds$ is a consequence of the stability which is already established in Step 3. We refer to [20, 44] for this technical proof. Thus, we have proved assertion (i), which states that $q : [0, T] \rightarrow Q$ is a solution.

Step 6: Improved convergence. Having energy equality, we conclude that in (65) all the inequalities must be equalities. In particular, this implies

$$\mathfrak{p}(t) = \mathfrak{P}(t), \quad \mathfrak{G}(t) = G^0(t, q(t)) \quad \text{and} \quad \text{Var}(q; 0, t) = \mathfrak{D}(t). \quad (67)$$

Together with the convergence properties established in Step 2, we obtain the assertions (iii)–(v). \square

Remark 5.9 Time-varying Dirichlet boundary conditions that would model a “hard-device” loading would need $u_D \in W^{1,1}(0, T; W^{1-1/p, p}(\Gamma_D; \mathbb{R}^3))$ and would make the proofs quite technical, exploiting nontrivial tricks from [20], see also [44].

6 Modelling of a stress-induced transformation in CuAlNi

CuAlNi is the second most popular SMA with a cheaper production cost than the number-one SMA, i.e. NiTi. Depending on composition, this sort of alloys exhibit large variations of transformation temperatures, even over 100°C. These Cu-based alloys undergo the *cubic-to-orthorhombic* (called also $\beta \rightarrow \gamma'_1$) PT as well as the *cubic-to-monoclinic* (called also $\beta_1 \rightarrow \beta'_1$ and $\beta_1 \rightarrow \beta''_1$) PT, depending on loading regimes and other circumstances. For example, experimental experience shows that the orthorhombic martensite mostly evolves in single crystals under compression, while the monoclinic one under tension. While the latter PT has a small hysteresis loop, the cubic-to-orthorhombic PT shows significant hysteresis. We opted for modelling of the cubic-to-orthorhombic transformation because of its smaller number of wells of $\hat{\varphi}$, the larger hysteresis, and because the elastic constants which are at disposal for the orthorhombic martensite contrary to the monoclinic one; cf. [69, 83]; even it should be emphasized that these constants, although routinely known for austenite, are not measured for any other SMA in martensite. First modelling studies with CuAlNi are probably by Falk and Konopka who formulated a 3D stored energy potential [19]. The laminated microstructure even with adaptive level of lamination have been used for CuAlNi by Aubri, Fago, and Ortiz [5] who also used (up to a factor 4) the potential (6)–(7) and by Stupkiewicz and Petryk [74]. A simplified model addressing CuAlNi is by Abeyaratne, Chu, James [1], or Hall and Govindjee [28]. Crystallographic discourse is, e.g., in Bhattacharya [13] and Xiangyang and al. [82]. Experiments with CuAlNi single-crystals are e.g. due to Abeyaratne et al. [1], Novák et al. [52], Otsuka et al. [54], Sedláč et al. [69], Šittner et al. [72], Suezawa and Sumimo [75].

6.1 Stored-energy data

The atomic-grid *lattice constants* for the composition Cu-14.0wt%Al-4.2wt%Ni we have in mind for the cubic austenite is $a_0 = 0.5835\text{nm}$ while the orthorhombic martensite has the lattice constants $a = 0.43823\text{nm}$, $b = 0.53563\text{nm}$, and $c = 0.4223\text{nm}$; see [17] or also [54]. In terms of the distortion matrices, this results to the cubic austenitic phase having one orbit $\text{SO}(3)U_0$ with $U_0 = \mathbb{I}$ while the orthorhombic martensite has $M = 6$ variants, i.e. six orbits $\text{SO}(3)U_1, \dots, \text{SO}(3)U_6$,

with the distortion matrices given by

$$\begin{aligned}
U_1 &= \begin{pmatrix} \eta_2 & 0 & 0 \\ 0 & \eta_1 & \eta_3 \\ 0 & \eta_3 & \eta_1 \end{pmatrix}, & U_2 &= \begin{pmatrix} \eta_1 & 0 & \eta_3 \\ 0 & \eta_2 & 0 \\ \eta_3 & 0 & \eta_1 \end{pmatrix}, & U_3 &= \begin{pmatrix} \eta_1 & \eta_3 & 0 \\ \eta_3 & \eta_1 & 0 \\ 0 & 0 & \eta_2 \end{pmatrix}, \\
U_4 &= \begin{pmatrix} \eta_2 & 0 & 0 \\ 0 & \eta_1 & -\eta_3 \\ 0 & -\eta_3 & \eta_1 \end{pmatrix}, & U_5 &= \begin{pmatrix} \eta_1 & 0 & -\eta_3 \\ 0 & \eta_2 & 0 \\ -\eta_3 & 0 & \eta_1 \end{pmatrix}, & U_6 &= \begin{pmatrix} \eta_1 & -\eta_3 & 0 \\ -\eta_3 & \eta_1 & 0 \\ 0 & 0 & \eta_2 \end{pmatrix}, \quad (68)
\end{aligned}$$

where we used $\eta_1 = 1.04245$ and $\eta_2 = 0.9178$, $\eta_3 = 0.01945$ in agreement with measurements by Otsuka and Shimizu [54] on the considered Cu-14.0wt%Al-4.2wt%Ni; the same constants are also in Ball, Chu and James [9] for a slightly different composition, namely Cu-14.0wt%Al-3.9wt%Ni. The relations with the lattice constants are $\eta_1 = (a + c)/(\sqrt{2}a_0)$, $\eta_2 = b/a_0$, and $\eta_3 = (a - c)/(\sqrt{2}a_0)$, see e.g. [13].

Using the usual Voigt notation (and $\{\mathbb{C}_{ij}^\ell\}_{i,j=1}^6$ instead of the 4th-order tensor \mathbb{C}^ℓ from (6)), the energy (6) results to the quadratic form

$$\begin{aligned}
\hat{\varphi}_\ell(F) &= \frac{1}{2}\mathbb{C}_{11}^\ell[\varepsilon_{11}^\ell]^2 + \frac{1}{2}\mathbb{C}_{22}^\ell[\varepsilon_{22}^\ell]^2 + \frac{1}{2}\mathbb{C}_{33}^\ell[\varepsilon_{33}^\ell]^2 \\
&+ \mathbb{C}_{12}^\ell\varepsilon_{11}^\ell\varepsilon_{22}^\ell + \mathbb{C}_{13}^\ell\varepsilon_{11}^\ell\varepsilon_{33}^\ell + \mathbb{C}_{23}^\ell\varepsilon_{22}^\ell\varepsilon_{33}^\ell \\
&+ 2\mathbb{C}_{44}^\ell[\varepsilon_{23}^\ell]^2 + 2\mathbb{C}_{55}^\ell[\varepsilon_{13}^\ell]^2 + 2\mathbb{C}_{66}^\ell[\varepsilon_{12}^\ell]^2, \quad (69)
\end{aligned}$$

and gives the Cauchy stress $\sigma = \hat{\varphi}'_\ell(\varepsilon^\ell)$, i.e.

$$\begin{pmatrix} \sigma_{11} \\ \sigma_{22} \\ \sigma_{33} \\ \sigma_{23} \\ \sigma_{13} \\ \sigma_{12} \end{pmatrix} = \begin{pmatrix} \mathbb{C}_{11}^\ell & \mathbb{C}_{12}^\ell & \mathbb{C}_{13}^\ell & 0 & 0 & 0 \\ \mathbb{C}_{12}^\ell & \mathbb{C}_{22}^\ell & \mathbb{C}_{23}^\ell & 0 & 0 & 0 \\ \mathbb{C}_{13}^\ell & \mathbb{C}_{23}^\ell & \mathbb{C}_{33}^\ell & 0 & 0 & 0 \\ 0 & 0 & 0 & \mathbb{C}_{44}^\ell & 0 & 0 \\ 0 & 0 & 0 & 0 & \mathbb{C}_{55}^\ell & 0 \\ 0 & 0 & 0 & 0 & 0 & \mathbb{C}_{66}^\ell \end{pmatrix} \begin{pmatrix} \varepsilon_{11}^\ell \\ \varepsilon_{22}^\ell \\ \varepsilon_{33}^\ell \\ 2\varepsilon_{23}^\ell \\ 2\varepsilon_{13}^\ell \\ 2\varepsilon_{12}^\ell \end{pmatrix}. \quad (70)$$

If we denote the vector on the right-hand side by $\bar{\varepsilon}^\ell$ we easily see that $\hat{\varphi}_\ell(F) = \frac{1}{2}\bar{\varepsilon}^\ell \cdot \mathbb{C}^\ell \bar{\varepsilon}^\ell$.

The specific values are determined from experiments; we refer to Sedláč et al. [69]. For $\ell = 0$, i.e. for the austenite, by symmetry there are only 3 nonvanishing elastic moduli, i.e. here

$$\mathbb{C}_{11}^0 = \mathbb{C}_{22}^0 = \mathbb{C}_{33}^0 = 142.8 \text{ GPa}, \quad (71a)$$

$$\mathbb{C}_{44}^0 = \mathbb{C}_{55}^0 = \mathbb{C}_{66}^0 = 93.5 \text{ GPa}, \quad (71b)$$

$$\mathbb{C}_{12}^0 = \mathbb{C}_{23}^0 = \mathbb{C}_{13}^0 = 129.7 \text{ GPa}, \quad (71c)$$

see also (for nearly the same values) Landa et al [37] or Suezawa and Sumimo [75]. The specific values for martensite, measured by Sedláč et al. [69] or also (a slightly different alloy, namely Cu-14wt%Al-3wt%Ni) by Yasunaga et al. [83], are

$$\mathbb{C}_{11}^\ell = 189 \text{ GPa}, \quad \mathbb{C}_{22}^\ell = 141 \text{ GPa}, \quad \mathbb{C}_{33}^\ell = 205 \text{ GPa}, \quad (72a)$$

$$\mathbb{C}_{44}^\ell = 54.9 \text{ GPa}, \quad \mathbb{C}_{55}^\ell = 19.7 \text{ GPa}, \quad \mathbb{C}_{66}^\ell = 62.6 \text{ GPa}, \quad (72b)$$

$$\mathbb{C}_{12}^\ell = 124 \text{ GPa}, \quad \mathbb{C}_{13}^\ell = 45.5 \text{ GPa}, \quad \mathbb{C}_{23}^\ell = 115 \text{ GPa}, \quad (72c)$$

counted with respect to the co-ordinate system oriented in the atomic lattice of the prism $a \times b \times c$; the are the same for $\ell = 1, \dots, 6$. The specific rotations R_ℓ , $\ell = 1, \dots, 6$, involved in (6) are calculated from the equation $U_\ell = R_\ell H R_\ell^\top$, where $H = \text{diag}(\eta_1 + \eta_3, \eta_2, \eta_1 - \eta_3)$, namely:

$$\begin{aligned} R_1 &= \begin{pmatrix} 0 & 1 & 0 \\ s & 0 & s \\ s & 0 & -s \end{pmatrix}, & R_2 &= \begin{pmatrix} -s & 0 & -s \\ 0 & -1 & 0 \\ -s & 0 & s \end{pmatrix}, & R_3 &= \begin{pmatrix} s & 0 & s \\ s & 0 & -s \\ 0 & 1 & 0 \end{pmatrix}, \\ R_4 &= \begin{pmatrix} 0 & -1 & 0 \\ -s & 0 & -s \\ s & 0 & -s \end{pmatrix}, & R_5 &= \begin{pmatrix} s & 0 & s \\ 0 & 1 & 0 \\ -s & 0 & s \end{pmatrix}, & R_6 &= \begin{pmatrix} -s & 0 & -s \\ s & 0 & -s \\ 0 & -1 & 0 \end{pmatrix}. \end{aligned} \quad (73)$$

where $s = \sin(45^\circ) = \sqrt{2}$.

Furthermore, the offset d_ℓ in (6) has been chosen as 3 MPa. Taking into account that the equilibrium temperature of the austenite and martensite is in this particular alloy about 293 K and that the difference d_ℓ between free energies of unstressed austenite and martensite with the temperature at the rate 160 kPa/K, cf. [51] (which, roughly speaking, after being divided by a transformation strain, i.e. here about 6%, yields the so-called *Clausius-Clapeyron constant* about 2.7 MPa/K), the considered temperature of our experiment results to 312 K.

6.2 Dissipation-energy data

As to the construction of the phase-indicator function $\mathcal{L} : \mathbb{R}^{3 \times 3} \rightarrow \Delta$ we first calculate for a given $F \in \mathbb{R}^{3 \times 3}$ its right Cauchy-Green tensor $F^\top F$ and then evaluate the square of its Euclidean distance (i.e. Frobenius' norm $|\cdot|_F$) to $U_\ell^\top U_\ell$ for all $\ell = 0, \dots, M = 6$. Taking a smooth function $d : \mathbb{R} \rightarrow \mathbb{R}$ such that $d = 1$ in a neighborhood of 0 and $d = \delta$ otherwise for some $\delta > 0$ small, we can put

$$\hat{\mathcal{L}}(F) := \left\{ \frac{d(|F^\top F - U_\ell^\top U_\ell|_F^2)}{\sum_{l=0}^M d(|F^\top F - U_l^\top U_l|_F^2)} \right\}_{\ell=0}^M \in \Delta. \quad (74)$$

Note that $\hat{\mathcal{L}}$ is frame indifferent.

The dissipation potential R from (16) involves a norm $|\cdot|_M$ on \mathbb{R}^{1+M} which we take here simply as $|\lambda|_M = \sum_{\ell=0}^M \gamma_\ell |\lambda_\ell|$ where $\gamma_\ell > 0$ for all $0 \leq \ell \leq M$; for more general form

In terms of the PT-energies $\{\mathcal{E}_{\ell l}\}_{\ell, l=0, \dots, M}$, see Section 4, this setting corresponds to the specific dissipation energy $\mathcal{E}_{\ell l} = \gamma_\ell + \gamma_l$ if $\ell \neq l$ (otherwise $\mathcal{E}_{\ell l} = 0$). We can see that we cannot set up these energies entirely arbitrarily, which is due to a simple choice of $|\cdot|_M$; for a more general choice $|\lambda|_M := \max_{\omega \in Z} \omega \cdot \lambda$ with Z a polyhedron determining activation stress of particular PTs (cf. (21)) we refer to [48]. We take $\gamma_0 = 0.5$ MPa (cf. [51]) and $\gamma_\ell = 1$ Pa for $\ell \neq 1, \dots, M = 6$. This choice of γ 's leads here to

$$\mathcal{E}_{\ell l} \doteq \begin{cases} 0.5 \text{ MPa} & \text{for } l = 0 \text{ or } \ell = 0, \ell \neq l, \\ 0 & \text{otherwise,} \end{cases} \quad (75)$$

i.e. transformations between the austenite and any martensitic variant need (and dissipate) the specific energy 0.5 MJ/m³ while reorientation of martensite in almost non-dissipative. The higher austenite-martensite dissipation is in agreement with

an observation by James and Zhang [32] that the transformation between rank-one connected austenite and martensite dissipates significantly less than if there is no rank-one connection, which is just our case and it corresponds to the option (A) in Section 4. Moreover, experimental observations due to Abeyratne et al. [1] show, however, also fairly wide hysteresis loop in the stress/volume fraction diagram during the reorientation of the martensitic variant 3 to 6 which are rank-one connected and which perhaps suggest also a non-vanishing dissipation in this case, which suggests also the option (B) in Section 4 to be considered additionally to (A).

6.3 Design of a particular experiment and computer implementation

Consistently with Section 5, we implemented the 3D-situation by using piecewise *affine tetrahedral finite elements* with a standard division of a prism into five tetrahedrons. This means that $\nabla u_{\tau,h}^k$ is element-wise constant, cf. (33). We implemented the *second-order laminate*, i.e. we put $\kappa = 2$ which leads to the four-atomic Young measure ν , cf. (3) and Figure 2, where

$$\nu_h = \xi_{0h}\xi_{1h}\delta_{F_{1h}} + \xi_{0h}(1-\xi_{1h})\delta_{F_{2h}} + (1-\xi_{0h})\xi_{2h}\delta_{F_{3h}} + (1-\xi_{0h})(1-\xi_{2h})\delta_{F_{4h}}, \quad (76)$$

with

$$F_{1h} = \nabla u_h - (1-\xi_{0h})a_h \otimes n_h - (1-\xi_{1h})a_{1h} \otimes n_{1h}, \quad (77a)$$

$$F_{2h} = \nabla u_h - (1-\xi_{0h})a_h \otimes n_h + \xi_{1h}a_{1h} \otimes n_{1h}, \quad (77b)$$

$$F_{3h} = \nabla u_h + \xi_{0h}a_h \otimes n_h - (1-\xi_{2h})a_{2h} \otimes n_{2h}, \quad \text{and} \quad (77c)$$

$$F_{4h} = \nabla u_h + \xi_{0h}a_h \otimes n_h + \xi_{2h}a_{2h} \otimes n_{2h}. \quad (77d)$$

Here $0 \leq \xi_{ih} \leq 1$, $i = 0, 1, 2$, are element-wise constant. The vectors a_{ih} and n_{ih} are element-wise constant as well and, moreover, we may choose $|n_{ih}| = 1$ and write it in spherical coordinates. Hence, the whole Young measure ν is identified by means of ∇u_h and $\{\xi_{ih}, a_{ih}, n_{ih}\}$.

Our specimen is a prism $\Omega := (0, 4) \times (0, 9) \times (0, 4)$ (in mm's) and the orientation of the crystal lattice is considered (001). The displacement $u(x)$ is prescribed to be zero on the bottom base, i.e. if $x \in \Gamma_D = (0, 4) \times \{0\} \times (0, 4)$. The specimen is subjected to a time-periodic surface force f independent of the deformation. This force is applied on the upper base of the specimen, i.e., if $x \in \Gamma_N = (0, 4) \times \{9\} \times (0, 4)$.

We used 180 tetrahedral elements, cf. Figure 4, which yields 3480 variables and 540 box constraints.

The resulted mathematical-programming problem (35) is solved by the optimization routine ‘‘L-BFGS-B’’ described in [16]. Due to the multi-well character of $\hat{\varphi}$, (35) is a nonconvex nonsmooth (due to the nonsmoothness of the dissipation metric $|\cdot|_M$) minimization problem, which, together with rather big number of variables, makes finding a global minimum extremely difficult. As ‘‘L-BFGS-B’’ is designed for local optimization, we need some strategy to rule out at least some of local minima. Successful (at least partly) computations are conditioned by a good initial guess at each time level k . Our initial guess heavily relies on possible rank-one connection between variants or their laminated mixtures. Above all, we see that $\text{SO}(3)U_l$ is not rank-one connected to $\text{SO}(3)$ if $l > 0$. As all U_l are symmetric this can be shown by looking at middle eigenvalues of U_l , $l > 0$; cf. [12]. We easily see that no middle eigenvalue is equal to 1. However, there are rank-one connections between the austenite and a twinned martensite. We exploit them for getting a initial guess in our calculations. For each two martensitic wells we calculate the appropriate rank-one connections (there always exist 2 such connections; cf. [14]). Having a matrix

$F_{l\ell}$ such that $F_{l\ell} = \tilde{\xi}R_lU_l + (1 - \tilde{\xi})R_\ell U_\ell$, where $R_lU_l - R_\ell U_\ell$ has the rank equal to one and $0 < \tilde{\xi} < 1$, we find $\tilde{\xi}$ and rotations R_l and R_ℓ such that $\text{SO}(3)F_{l\ell}$ is rank-one connected to $\text{SO}(3)$, i.e. to the well of the austenite. This precisely means that $F_{l\ell}^T F_{l\ell}$ has positive eigenvalues and the middle one is equal to 1. A very important piece of information coming from these calculations are normal vectors of laminates between martensitic variants and the twinned martensite and the austenite., i.e., n_h, n_{1h} , and n_{2h} . We use them as possible starting points during our computational experiments. After evaluating corresponding discrete energies, we pick up a solution with the least energy.

Notice that, since we use a second-order laminate, i.e. $\kappa = 2$ and thus a pairwise rank-1-connected four-atomic probability measure, we can reach certain microstructures consisting of no more than four material phases/variants like on Figure 1e without necessity of fast spatial oscillations which would hardly be approached on our quite coarse discretizations. The initial condition is chosen so that $u_0 = 0$ and $[\nu]_0 = \delta_0$, i.e., the stress-free austenite.

However, we dared commit three shortcomings: we eventually did not implement the regularization by (26) of V (and put $\rho = 0$ in (24)), we did not implement the penalization in (34) (and took simply $\lambda = \mathcal{L} \bullet \nu$), and we did not treat the absolute value in the metric $|\cdot|_M$ in the dissipation potential as nonsmooth but, just for numerical reasons, we replaced it by its regularization $|y| \approx \sqrt{y^2 + \beta}$ with $\beta = 10^{-8}$ which makes the mathematical-programming problem (35) smooth although ill-conditioned as β is small.

6.4 Computer simulations of a compression experiment

As already mentioned, the orthorhombic martensite is more likely to appear during a compression experiment. We implemented the loading $f(\cdot, x) = (0, f_2(\cdot, x), 0)$ having a saw-tooth profile in time. Its amplitude is 10.8 kN, which reflects the maximal compressive stress 300 MPa. The obtained stress-strain diagram in on Figure 3.

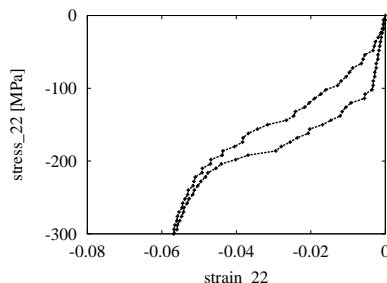


Fig. 3. The hysteretic pseudo-elastic stress-strain response corresponding to the full loading/unloading cycle.

We can observe that the area of the hysteresis loop is close to 1 MPa which is twice the preset value from (75) corresponding to two PTs from austenite to martensite and back, although it is not accomplish fully in the whole bulk.

In this particular experiment, we observed only three wells really active which causes that only at most three-atomic Young measures had been observed during the simulation; i.e. the nodes (or leaves) F_3 and F_4 (or equally F_1 and F_2) on Figures 2 coincide with each other. From the calculated values of ξ 's, a 's, and n 's in (3), we can *a-posteriori* reconstruct a microstructure (or, more precisely, minimizing sequences for (35) which are schematically displayed in circles on Figures 4 and 5 recording volume fractions ξ 's and orientation of interfaces n 's but not the amplitudes a 's. We

can observe interfaces between the austenite (called *habit planes*) and the *twinning planes* (cf. Figure 1c) in the twinned martensite.

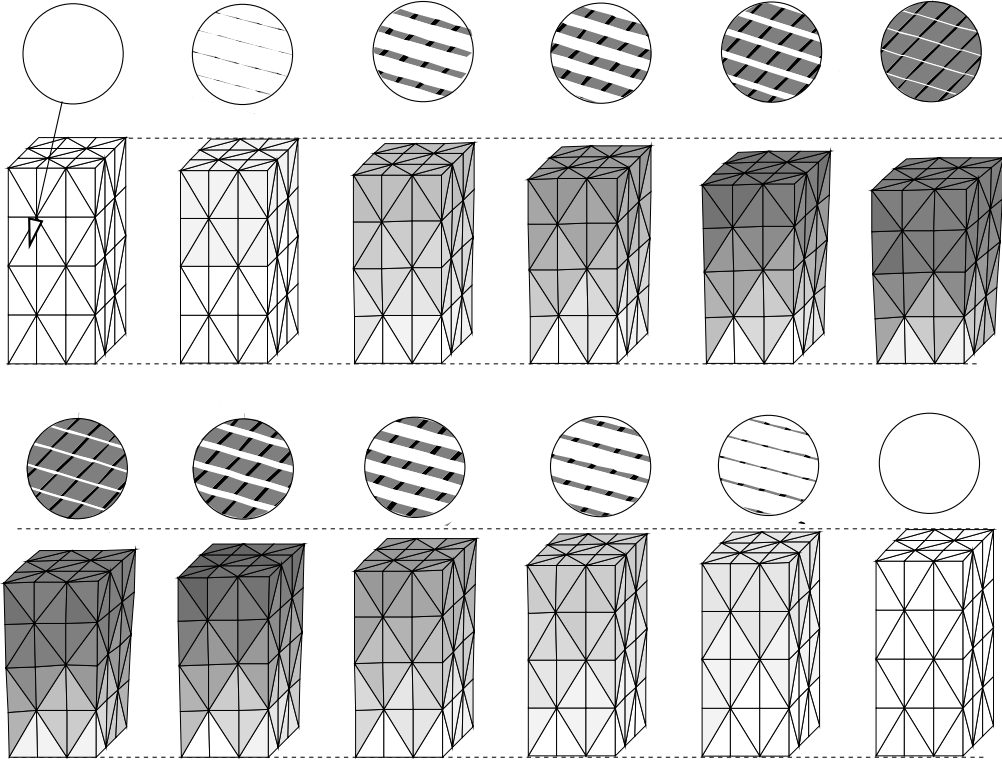


Fig. 4. Evolution of a 2nd-order laminated microstructure in cubic/orthorhombic austenite/martensite stress-induced transformation at one selected spot of a loaded CuAlNi (001)-oriented single-crystal. Austenite (white) transforms through 2 variants (U_2 =gray and U_3 =black) of twinned martensite to a single variant of (so-called de-twinned) martensite. A dozen of snapshots covers the whole loading (upper row) and unloaded (lower row) cycle corresponding to Figure 3. Microstructure is reconstructed in accord with calculations on one selected element. The gray level in the specimen reflects the calculated volume fraction of the “mixture” of the martensitic variants 2 and 3 and the austenite, i.e. the deformation gradient is in neighborhoods of $\text{SO}(3)U_2$, $\text{SO}(3)U_3$ and $\text{SO}(3)U_0$, respectively. The displacement is magnified $3x$.

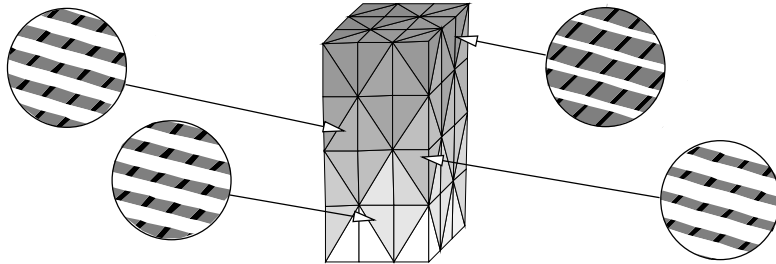


Fig. 5. One snapshot with microstructure displayed at several spots, showing a spatial inhomogeneity of the PT processes.

We finish the presentation of this experiment by displaying how selected quantities, namely energies (on Fig. 6) and volume fractions (on Fig. 7), evolve in time.

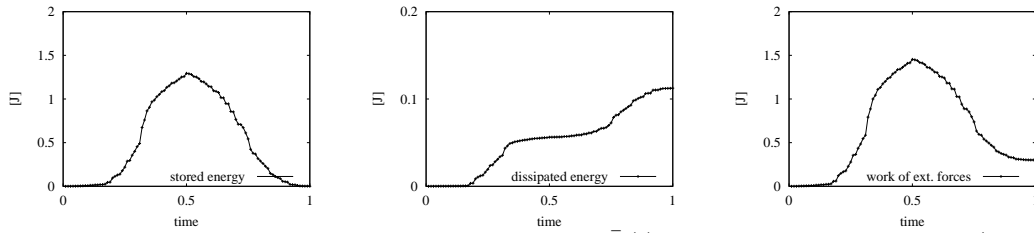


Fig. 6. Evolution of the Helmholtz stored energy $\bar{V}(t)$ and the dissipated energy (both in the whole specimen), and the work of external forces $\int_0^t \langle f, \frac{d}{dt} u \rangle dt$, cf. (19).

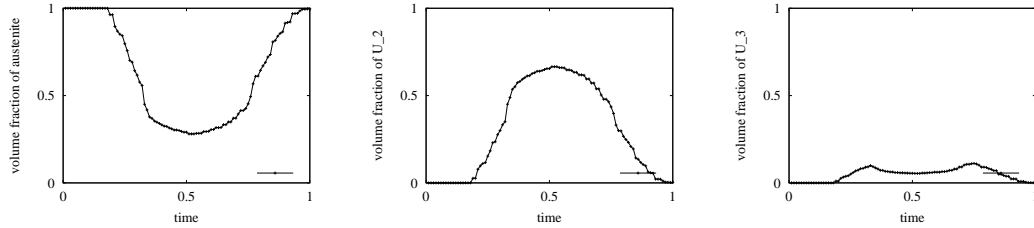


Fig. 7. Evolution of volume fractions averaged over the whole specimen of the austenite (left), the variant U_2 (middle) and the variant U_3 (right); the other variants were nonactive.

Due to the boundary conditions on the bottom side, the lower part of the single crystal cannot undergo the PT, see Fig. 4, which is why about 25% of austenite remains in the bulk even under extremely compressed specimen, see Fig. 7(left).

Acknowledgements.

The authors are indebted to M. Landa, V. Novák, P. Sedlák, P. Šittner, and U. Stefanelli for helpful discussions, and acknowledge the partial support from the European grants HPRN-CT-2002-00284 “Smart systems” and MRTN-CT-2004-505226 “Multi-scale modelling and characterisation for phase transformations in advanced materials”. Besides, M.K. is thankful for the support from the grants A 1075402 (GA AV ČR) and VZ 6840770021 (MŠMT ČR) and A.M. was also supported through C7-subproject of SFB 404 “Multifield Problems” and C18-subproject of the Research center “Matheon” (both Deutsche Forschungsgemeinschaft), while T.R. recognizes the support also from the grants 201/03/0934 (GA ČR) and MSM 0021620839 (MŠMT ČR). Last but not least, T.R. warmly acknowledges the support from the Alexander von Humboldt Foundation during his stay at the Weierstrass Institute, Berlin.

References

- [1] Abeyaratne R., Chu C., James R.D. Kinetics of materials with wiggly energies: Theory and application to the evolution of twinning microstructures in a Cu-Al-Ni shape memory alloy. *Phil. Mag. A* **73** (1996) 457-497.
- [2] Abeyaratne, R., Knowles, J.K.: On the propagation of maximally dissipative phase boundaries in solids. *Q. Appl. Math.* **50** (1992), 149–172.
- [3] Arndt, M.: Upscaling from Atomistic Models to Higher Order Gradient Continuum Models for Crystalline Solids. PhD.Thesis, Inst. für Numer. Simulation, Universität Bonn, 2004.

- [4] Arndt, M., Griebel, M., Novák, V., Roubíček, T., Šittner, P.: Martensitic transformation in NiMnGa single crystals: numerical simulations and experiments. *Int. J. Plasticity*, submitted.
- [5] Aubri, S., Fago, M., Ortiz, M.: A constrained sequential-lamination algorithm for the simulation of sub-grid microstructure in martensitic materials. *Comp. Meth. in Appl. Mech. Engr.* **192** (2003), 2823–2843.
- [6] Auld, B.A. : *Acoustic Fields and Waves in Solids*. Vol I. J. Wiley & Sons, New York, 1973.
- [7] Auricchio, F., Petrini, L.: A three-dimensional model describing stress-temperature induced solid phase transformations: solution algorithm and boundary value problems. *Int. J. Numer. Methods Engrg.* **61** (2004), 807–836.
- [8] Auricchio, F., Taylor, R.L., Lubliner, J.: Shape-memory alloys: macromodelling and numerical simulations of the superelastic behaviour. *Comp. Meth. Appl. Mech. Engr.* **146** (1997), 281–312.
- [9] Ball, J.M., Chu, C., James, R.D.: Hysteresis during stress-induced variant rearrangement. *J. de Physique IV (C8)* **5** (1995), 245–251.
- [10] Ball, J.M., Holmes, P.J., James, R.D., Pego, R.L., Swart P.J.: On the dynamics of fine structure. *J. Nonlinear Science* **1** (1991), 17–70.
- [11] Ball, J.M., James, R.D.: Fine phase mixtures as minimizers of energy. *Archive Rat. Mech. Anal.* **100** (1988), 13–52.
- [12] Ball, J.M., James, R.D.: Proposed experimental tests of a theory of fine microstructure and the two-well problem. *Phil. Trans. Royal Soc. London A* **338** (1992), 389–450.
- [13] Bhattacharya, K.: *Microstructure of martensite. Why it forms and how it gives rise to the shape-memory effect*. Oxford Univ. Press, New York, 2003.
- [14] Bhattacharya, K., Li, B., Luskin, M.: Uniqueness and stability of the simply laminated microstructure for martensitic crystals that undergo a cubic to orthorhombic phase transformation. *Archive Rat. Mech. Anal.* **149** (1999), 123–154.
- [15] Bhattacharya, K., Purohit, P., Craciun, B.: Mobility of twin and phase boundaries. *Journal de Physique IV* **112** (Proc. ICOMAT-02), 2003, 163-166.
- [16] Byrd, R.H., Lu, P., Nocedal, J., Zhu, C.: A limited memory algorithm for bound constrained optimization, *SIAM J. Scientific Computing* **16** (1995), 1190–1208.
- [17] Duggin, M.J., Rachinger, W.A.: The nature of the martensite transformation in a coppernickel-aluminium alloy. *Acta. Metal.* **12** (1964), 529
- [18] Eve, R.A., Reddy, B.D., Rockafellar, R.T.: An internal variable theory of elastoplasticity based on the maximum plastic work inequality. *Quarterly Appl. Math.* **48** (1990), 59–83.
- [19] Falk, F., Konopka, P.: Three-dimensional Landau theory describing the martensitic phase transformation of shape-memory alloys. *J. Condens. Matter* **2** (1990), 61-77.
- [20] Francfort, G., Mielke, A.: An existence result for a rate-independent material model in the case of nonconvex energies. *J. reine u. angew. Math.*, accepted.
- [21] Frémond, M.: *Non-Smooth Thermomechanics*. Springer, Berlin, 2002.
- [22] Frémond, M., Miyazaki, S.: *Shape memory alloys*. Springer, Wien, 1996.
- [23] Goldstein, G.H.: The effective energy and laminated microstructure in martensitic phase transformations. *J. Mech. Phys. Solids* **49** (2001), 899–925.
- [24] Govindjee, S., Miehe, C.: A multi-variant martensitic phase transformation model: formulation and numerical implementation. *Comp. Met. in Appl. Mech. Eng.* **191** (2001), pp. 215-238.

- [25] Govindjee, S., Mielke, A., Hall, G.J.: Free-energy of mixing for n -variant martensitic phase transformations using quasi-convex analysis. *J. Mech. Physics Solids* **50** (2002) 1897–1922.
- [26] Govindjee, S., Mielke, A., Hall, G.J., Miehe, C.: Application of notions of quasi-convexity to the modeling and simulation of martensitic and shape memory phase transformations. In: *Proc. 5th World Congress on Computational Mechanics*, (H.A. Mang, F.G. Rammerstorfer, J. Eberhardsteiner, Eds), Vienna University of Technology, Austria, (2002)
- [27] Hackl, K., Hoppe, U.: On the calculation of microstructure for inelastic materials using relaxed energies. In: *IUTAM Symp. Comput. Mech. of Solid Materials at Large Strains* (Ch.Miehe ed.), Kluwer, Dordrecht, 2003, pp.77–86
- [28] Hall, G.J., Govindjee, S.: Application of the relaxed free energy of mixing to problems in shape memory alloy simulation. *J. Intelligent Mater. Systems & Struct.*, in print.
- [29] Hill, R.: A variational principle of maximum plastic work in classical plasticity. *Q. J. Mech. Appl. Math.* **1** (1948), 18–28.
- [30] Huo, Y., Müller, I.: Nonequilibrium thermodynamics of pseudoelasticity. *Continuum Mech. Thermodyn.* **5** (1993), 163–204.
- [31] James, R.D., Hane, K.F.: Martensitic transformations and shape-memory materials. *Acta Mater.* **48** (2000), 197–222.
- [32] James, R.D., Zhang, Z.: A way to search for multiferroic materials with “unlikely” combination of physical properties. In: *Interplay of Magnetism and Structure in Functional Materials*. (L.Manoza et al., eds.), Springer, 2004.
- [33] Kristensen, J.: On the non-locality of quasiconvexity. *Ann. Inst. H. Poincaré Anal. Non Linéaire* **16** (1999), 1–13.
- [34] Kružík, M.: Numerical approach to double-well problem. *SIAM J. Numer. Anal.* **35** (1998), 1833–1849.
- [35] Kružík, M., Luskin, M.: The computation of martensitic microstructure with piecewise laminates. *J. Sci. Comp.* **19** (2003), 293–308.
- [36] Kružík, M., Roubíček, T.: Mesoscopic model of microstructure evolution in shape memory alloys with applications to NiMnGa. Preprint IMA No.2003, Univ.of Minnesota, Minneapolis, November 2004.
- [37] Landa, M., Plešek, J., Urbánek, P., Novák, V. Evaluation of anisotropic elastic properties by ultrasonic methods. In: *Proc. 40th Intl. Conf. Experimental Stress Anal., Prague, June 3–6, 2002*, pp. 141–146.
- [38] Levitas, V.I.: The postulate of realizability: formulation and applications to postbifurcational behavior and phase transitions in elastoplastic materials. *Int. J. Eng. Sci.* **33** (1995), 921–971.
- [39] LExcellent, C., Moyne, S., Ishida, A., Miyazaki, S.: Deformation behaviour associated with the stress-induced martensitic transformation in Ti-Ni thin films and their thermodynamical modelling. *Thin Solid Films* **324** (1998), 184–189.
- [40] Lubliner J.: A maximum dissipation principle in generalized plasticity. *Acta Mech.* **52** (1984), 225–237.
- [41] Mainik, A., Mielke, A.: Existence results for energetic models for rate-independent systems. *Calc. Var.* **22** (2005) 73–99.
- [42] Mielke, A.: Energetic formulation of multiplicative elastoplasticity using dissipation distances. *Cont. Mech. Thermodyn.* **15** (2003), 351–382.

- [43] Mielke, A.: Evolution of rate-independent inelasticity with microstructure using relaxation and Young measures. In: IUTAM Symp. *Comput. Mech. of Solid Mater. at Large Strains* (C.Miehe ed.), Kluwer, Dordrecht, 2003, pp. 33–44.
- [44] Mielke, A.: Evolution of rate-independent systems. In: *Handbook of Differential Equations: Evolutionary Diff. Eqs.* (Eds. C.Dafermos, E.Feireisl), North-Holland, Amsterdam, 2005, in print.
- [45] Mielke, A., Roubíček, T.: Rate-independent model of inelastic behaviour of shape-memory alloys. *Multiscale Modeling Simul.* **1** (2003), 571–597.
- [46] Mielke, A., Theil, F.: A mathematical model for rate-independent phase transformations with hysteresis. In: *Models of continuum mechanics in analysis and engineering.* (Eds.: H.-D.Alder, R.Balean, R.Farwig), Shaker Verlag, Aachen, 1999, pp.117–129.
- [47] Mielke, A., Theil, F.: On rate-independent hysteresis models. *Nonlin. Diff. Eq. Appl.* **11** (2004) 151–189.
- [48] Mielke, A., Theil, F., Levitas, V.I.: A variational formulation of rate-independent phase transformations using an extremum principle. *Archive Rat. Mech. Anal.* **162** (2002), 137–177.
- [49] Müller, I., Xu, H.: On the pseudoelastic hysteresis. *Acta Metall. Mater.* **39** (1991), 261–271.
- [50] Müller, S.: Variational models for microstructure and phase transitions. (Eds.: S.Hildebrandt et al.) *Lect. Notes in Math.* **1713** (1999), Springer, Berlin, pp.85–210.
- [51] Novák, V., Šittner, P.: Personal communication.
- [52] Novák, V., Šittner, P., Vokoun, D., Zárubová, N.: On the anisotropy of martensitic transformation in Cu-based alloys. *Mater. Sci. Eng.* **A273-275** (1999), 280–285.
- [53] Nicolaides, R.A., Walkington, N.J.: Computation of microstructure utilizing Young measure representations. In: *Recent Advances in Adaptive and Sensory Materials and their Applications.* (C.A.Rogers, R.A.Rogers, eds.) Technomic Publ., Lancaster, 1992, pp.131–141.
- [54] Otsuka, K., Shimizu, K.: Morphology and crystallography of thermoelastic Cu-Al-Ni martensite analyzed by the phenomenological theory. *Trans. Japan Inst. Metals* **15** (1974), 103–113.
- [55] Patoor, E., Eberhardt, A. Berveiller, M.: Micromechanical modelling of shape memory alloys behaviour. *Arch. Mech.* **40** (1988), 775–794.
- [56] Pedregal, P.: *Parametrized Measures and Variational Principles.* Birkhäuser, Basel, 1997.
- [57] Pitteri, M., Zanzotto, G.: *Continuum Models for Phase Transitions and Twinning in Crystals.* Chapman & Hall, Boca Raton, 2003.
- [58] Plecháč, P., Roubíček, T.: Visco-elasto-plastic model for martensitic phase transformation in shape-memory alloys. *Math. Methods Appl. Sci.* **25** (2002), 1281–1298.
- [59] Rajagopal, K.R., Roubíček, T.: On the effect of dissipation in shape-memory alloys. *Nonlinear Anal., Real World Appl.* **4** (2003), 581–597.
- [60] Rajagopal, K.R., Srinivasa, A.R.: On the inelastic behavior of solids – Part 1: Twinning. *Int. J. Plasticity* **11** (1995), 653–678.
- [61] Ren, X., Truskinovsky, L.: Finite scale microstructures in nonlocal elasticity. *J. Elasticity* **59** (2000), 319–355.
- [62] Rogers, R., Truskinovsky, L.: Discretization and hysteresis. *Physica B* **233** (1997), 370–375.

- [63] Roubíček, T.: A note on an interaction between penalization and discretization. In: *Modelling and Inverse Problems of Control for Distributed Parameter Systems*. (A.Kurzahnski, I.Lasiecka, eds.) L.N. in Control and Inf. Sci. **154**, Springer, Berlin, 1991, pp.145-150.
- [64] Roubíček, T.: *Relaxation in Optimization Theory and Variational Calculus*. W. de Gruyter, Berlin, 1997.
- [65] Roubíček, T.: Dissipative evolution of microstructure in shape memory alloys. In: *Lectures on Applied Mathematics*. (H.-J. Bungartz, R. H. W. Hoppe, C. Zenger, eds.) Springer, Berlin, 2000, pp.45-63.
- [66] Roubíček, T.: Evolution model for martensitic phase transformation in shape-memory alloys. *Interfaces and Free Boundaries* **4** (2002), 111-136.
- [67] Roubíček, T.: Models of microstructure evolution in shape memory materials. In: NATO Workshop *Nonlinear Homogenization and its Appl. to Composites, Polycrystals and Smart Mater.* (Eds. P.Ponte Castaneda, J.J.Telega, B.Gambin), NATO Sci. Series **II/170**, Kluwer, Dordrecht, 2004, pp.269-304.
- [68] Roubíček, T., Kružík, M.: Mesoscopic model of microstructure evolution in shape memory alloys, its numerical analysis and computer implementation. 3rd GAMM *Seminar on microstructures*. (Ed.C.Miehe), *GAMM Mitteilungen*, J.Wiley, in print.
- [69] Sedlák, P., Seiner, H., Landa, M., Novák, V., Šittner, P., Mañosa, LL.: Elastic constants of bcc austenite and 2H orthorhombic martensite in CuAlNi shape memory alloy. *Acta Mat.* (2005).
- [70] Šilhavý, M.: On the hysteresis in martensitic transformations. In: *Rational Continua, Classical and New*. (P. Podio-Guidugli, M. Brocato eds.), Springer, Berlin, 2003, pp.151-168.
- [71] Simo, J.C.: A framework for finite strain elastoplasticity based on maximum plastic dissipation and the multiplicative decomposition. *Comp. Math. Appl. Mech. Engrg.* **66** (1988), 199-219, **68** (1988), 1-31.
- [72] Šittner, P., Hashimoto, K., Kato, M., Tokuda, M.: Stress induced martensitic transformations in tension/torsion of CuAlNi single crystal tube. *Scripta Mater.* **48** (2003), 1153-1159.
- [73] Souza, A.C., Mamiya, E.N., Zouain, N.: Three-dimensional model for solids undergoing stress-induced phase transitions. *Eur. J. Mech. A/Solids* **15** (1998), 789-806.
- [74] Stupkiewicz, S., Petryk, H.: Modelling of laminated microstructures in stress-induced martensitic transformations. *J. Mech. Phys. Solids* **50** (2002), 2303-2331.
- [75] Suezawa, M., Sumimo, K.: Behaviour of elastic constants in Cu-Al-Ni alloy in the close vicinity of M_s -point. *Scr. Metall.* **10** (1976), 789-792.
- [76] Šverák, V.: Rank-one convexity does not imply quasiconvexity. *Proc. R. Soc. Edinb.* **120 A** (1992), 185-189.
- [77] Thamburaja, P., Anand, L.: Thermomechanically coupled superelastic response of initially-textured TiNi sheet. *Acta Mater.* **51** (2003), 325-338.
- [78] Truskinovsky, L.: Transition to detonation in dynamic phase changes. *Archive Rat. Mech. Anal.* **125** (1994), 375-397.
- [79] Vainchtein, A., Rosakis, P.: Hysteresis and stick-slip motion of phase boundaries in dynamic models of phase transitions. *J. Nonlin. Sci.* **9** (1999), 697-719.
- [80] Vivet, A., Lexcellent, C.: Micromechanical modelling for tension-compression pseudoelastic behaviour of AuCd single crystals. *Euro Phys.J. A.P.4* (1998), 125-132.
- [81] Wilmanski, K.: Symmetric model of stress-strain hysteresis loops in shape memory alloys. *Int. J. Engr. Sci.* **31** (1993), 1121-1138.

- [82] Xiangyang, Z., Qingping, S., Shouwen, Y.: A non-invariant plane model for the interface in CuAlNi single crystal shape memory alloys. *J. Mech. Phys. Solids* **48** (2000), 2163–2182.
- [83] Yasunaga, M., Funatsu, Y., Kojima, S., Otsuka, K., Suzuki, T.: Measurement of elastic constants. *Scr. Metall.* **17** (1983), 1091.
- [84] Zhang, X.Y., Brinson, L.C., Sun, Q.P.: The variant selection criteria in single-crystal CuAlNi shape memory alloys *Smart Materials and Structures* **9** (2000), 571-581.